AD-A176 238 CHARACTERIZING THERMAL/MECHANICAL PROPERTIES OF FILAMENT WOUND COMPOSITES(U) ARMY MILITARY PERSONNEL CENTER ALEXANDRIA VA B K FINK 15 JAN 87 1/1

UNCLASSIFIED F/G 11/4 NL

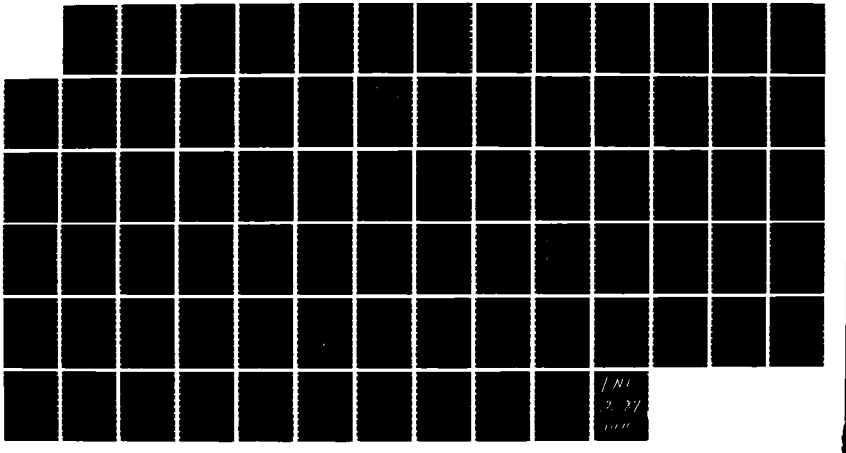

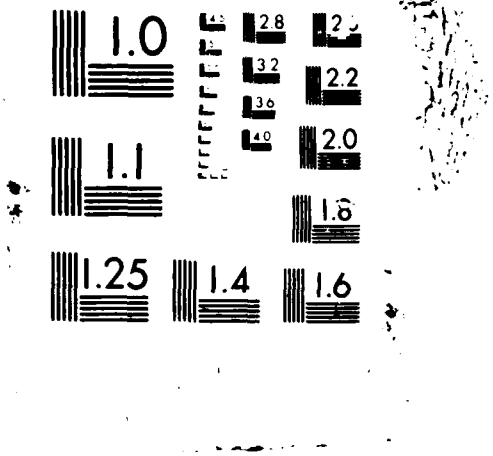
1.0
1.1
1.25
1.4
1.6
2.8
3.2
3.6
4.0
2.2
2.0
1.8

AD-A176 238

CHARACTERIZING THERMAL/MECHANICAL PROPERTIES OF FILAMENT WOUND COMPOSITES

2LT BRUCE K. FINK
HODA, MILPERCEN (DAPC-OPA-E)
200 Stovall Street
Alexandria, VA 22332

Final Report 15 JAN 87

Approved for public release;
distribution is unlimited

A thesis submitted to
The Graduate College of the University of Nebraska
Lincoln, Nebraska
In partial fulfillment of the requirements for the degree of
Master of Science in Engineering

SECURITY CLASSIFICATION OF THIS PAGE (When Data Entered)

REPORT DOCUMENTATION PAGE		READ INSTRUCTIONS BEFORE COMPLETING FORM
1 REPORT NUMBER	2. GOVT ACCESSION NO.	3 RECIPIENT'S CATALOG NUMBER
4. TITLE (and Subtitle) CHARACTERIZING THERMAL MECHANICAL PROPERTIES OF FILAMENT WOUND COMPOSITES		5 TYPE OF REPORT & PERIOD COVERED Final Report 15 JAN 87
		6 PERFORMING ORG. REPORT NUMBER
7. AUTHOR(s) 2LT BRUCE K. FINK		8 CONTRACT OR GRANT NUMBER(s)
9. PERFORMING ORGANIZATION NAME AND ADDRESS Student, HQDA, MILPERCEN (DAPC-OPA-E), 200 Stovall Street, Alexandria, Virginia 22332		10 PROGRAM ELEMENT, PROJECT, TASK AREA & WORK UNIT NUMBERS
11. CONTROLLING OFFICE NAME AND ADDRESS HQDA, MILPERCEN, ATTN: DAPC-OPA-E, 200 Stovall St. Alexandria, Virginia 22332		12. REPORT DATE 15 JAN 87
		13 NUMBER OF PAGES 75
14. MONITORING AGENCY NAME & ADDRESS(if different from Controlling Office)		15. SECURITY CLASS. (of this report)
		15a. DECLASSIFICATION DOWNGRADING SCHEDULE

16. DISTRIBUTION STATEMENT (of this Report)
Approved for public release; distribution unlimited.

17. DISTRIBUTION STATEMENT (of the abstract entered in Block 20, if different from Report)

18. SUPPLEMENTARY NOTES
A thesis submitted to the University of Nebraska, Lincoln, NE 68508 in partial fulfillment of the requirements for the degree of Master of Science in Engineering.

19. KEY WORDS (Continue on reverse side if necessary and identify by block number)
thermal, mechanical, coefficient of expansion, filament, wound, composite, delamination, residual stresses, S2-Glass/Epoxy, AS4 Graphite/Epoxy, finite element, ANSYS

20. ABSTRACT (Continue on reverse side if necessary and identify by block number)
The characterization of composites is a continuing process involving a wide variety of materials with different compositions, laminate geometries and fabrication processes. This thesis examines bench test methods for the determination of the linear coefficients of thermal expansion, residual stresses due to fabrication, and delamination strengths in S2-Glass/Epoxy and AS4 Graphite/Epoxy filament wound cylinders. Results from these tests are compared to finite element and closed form solutions. Test theory correlation is generally good. The slopes of temperature-strain curves are closely approximated by the linear

DD FORM 1 JAN 73 1473 EDITION OF 1 NOV 65 IS OBSOLETE

SECURITY CLASSIFICATION OF THIS PAGE (When Data Entered)

20.

coefficient of thermal expansion calculated for the laminates. Predicted values of residual stress are approximately equal to those determined by a simple bench test. Measured delamination strengths were found to be considerably lower (35%) than other published data.

CHARACTERIZING THERMAL/MECHANICAL PROPERTIES OF FILAMENT WOUND COMPOSITES

by

Bruce K. Fink

A THESIS

Presented to the Faculty of
The Graduate College in the University of Nebraska
In Partial Fulfillment of Requirements
For the Degree of Master of Science

Major: Engineering Mechanics

Under the Supervision of Professor Ralph F. Foral

Lincoln, Nebraska

January, 1987

A-1

TABLE OF CONTENTS

CHARACTERIZING THERMAL/MECHANICAL PROPERTIES

OF FILAMENT WOUND COMPOSITES

Bruce Kendall Fink, M.S.

University of Nebraska, 1987

Advisor: Ralph F. Foral

The characterization of composites is a continuing process involving a wide variety of materials with different compositions, laminate geometries and fabrication processes. This thesis examines bench test methods for the determination of the linear coefficients of thermal expansion, residual stresses due to fabrication, and delamination strengths in S2-Glass/Epoxy and AS4 Graphite/Epoxy filament wound cylinders. Results from these tests are compared to finite element and closed form solutions. Test theory correlation is generally good. The slopes of temperature-strain curves are closely approximated by the linear coefficient of thermal expansion calculated for the laminates. Predicted values of residual stress are approximately equal to those determined by a simple bench test. Measured delamination strengths were found to be considerably lower (35%) than other published data.

ACKNOWLEDGEMENTS

This author sincerely thanks Professor Ralph Foral for his guidance and encouragement throughout the course of his graduate studies and the completion of this thesis. A special thank you is given for Donald Gilbreath and Lyle Ang for their support and advice. Appreciation is extended to Professors S.I. Chow and R.E. Ekstrom as members of this author's graduate committee. This thesis is dedicated to the author's ever-supportive wife, Lorie.

LIST OF TABLES

LIST OF FIGURES

SYMBOLS

1,2,3	ply material axes
A	surface area
[A]	in-plane stiffness matrix
α	linear coefficient of thermal expansion
act	subscript meaning actual
AVE	average value
[B]	in-plane/flexural coupling submatrix of a stiffness matrix for an unsymmetric laminate
CoC	coefficient of correlation
CoV	coefficient of variation
d	length of cylinder under effects of discontinuity
d	diameter
E	modulus of elasticity
ϵ	normal strain
γ	shear strain
ϵ_o	midlayer strain
^oF	degrees Fahrenheit
"gl"	inside S2 Glass/Epoxy hoop layer
"gr"	AS4 Graphite/Epoxy hoop helical layers
G	shear modulus
h_k	measurement through the thickness from inside to layer k
i,j	indicial subscripts for i,j = 1,2,6
k	curvature in general
k	subscript indicating "per layer"
K	curvature of half-ring specimens
m	cos
m,h,r	meridional, hoop, radial cylindrical structural reference axes used in the computer program TDCYL2
matl	subscript for quantities from the computer program MATL
n	sin
N	running load (lb/in)
$[N]^T$	stress resultant due to temperature change
[Q]	general stiffness matrix
$[\bar{Q}]$	transformed stiffness matrix
R_o	initial radius
R_f	final radius
r	radius in general
σ	normal stress
t	thickness of layer
ΔT	change in temperature
[T]	tensor transformation matrix
$[T]^{-1}$	inverse of [T]
τ	shear stress
θ	ply orientation angle from x-axis

CHAPTER 1 - INTRODUCTION

1.1 Background

A composite material can be defined as a materials system composed of a mixture or combination of two or more macroconstituents differing in form and/or material composition and that are essentially insoluble in each other. Generally, we consider advanced composites to be fiber-matrix composites. Even within this classification of composites there exist millions of possible final usable materials. Many complex processing variables control the quality and reliability or uniformity of composites. They relate both to the quality of the individual constituent elements and, often more important, to that involved when the constituents are combined into the finished composite. In many fiber composites, uniformity in orientation of the fibers, control of the matrix content, quality of the interfacial bonds, and many other processing variables influence the composite's performance directly.

Even if standards of quality and uniformity were perfect, there are still a vast number of possible fiber and matrix materials to choose from. Further, for every fiber-matrix pair there are an infinite number of laminate geometries. Given all these different materials, characterization of composite materials in general becomes a challenging task without an adequate unifying theory.

1.2 Goals of Thesis

To determine the strength and other properties of a particular composite researchers are forced to either compare it to a similar material for which characterization testing has already been accomplished or perform testing ourselves. Bert[1] recognized that simple bench tests are desirable in determining these properties. This thesis investigates methods for the determination of the linear coefficients of thermal expansion (Chapter 2), residual stresses due to fabrication (Chapter 3), and delamination strengths (Chapter 4) in S2-Glass/Epoxy and AS4 Graphite/Epoxy filament wound cylindrical composites.

The prediction of laminate properties from known or assumed fiber and matrix properties is also a difficult task. Another goal of this paper is to determine the applicability of the proprietary program ANSYS, a well-known general purpose finite element program, to the problems covered. An educational version of ANSYS was available at UNL on the VAX mainframe system. Finite element results are then compared to closed form solutions using other locally available programs.

1.3 Specimens and Properties

Experimental work began with tests being conducted in the Engineering Mechanics lab at UNL by Foral et.al.[2] with filament wound cylinders. Four different types of laminates were tested; two compression and two tension. All tubes were

wound on a 2.78 inch diameter mandrel with the compression specimens being cut to approximately 3" in length and the tension specimens being cut to approximately 14". Table 1.1 (next page) shows the various laminates, thicknesses, and wind angles. "Inner" refers to the all S2 Glass/Epoxy laminates while "outer" refers to the laminates with graphite helicals. Information concerning the "outer" tension tests significant to this thesis is the location of delamination. Large areas in the test section of the cylindrical specimens delaminated at failure consistently between the graphite/epoxy and glass/epoxy helical layers (Table 1.1).

Some of the specimens being tested in compression were cooled or heated to certain temperatures prescribed for the particular compression tests. As the opportunity presented itself, strain data was recorded during the change in temperature using an IBM PC Portable computer, Measurements Group 2100 System Signal Conditioner and Amplifier, Metrabyte Dash-8 A/D Converter, a program called DASHSOFT written by Gilbreath[3], and an Omega 2168A Digital Thermocouple device. This data was then used to determine a coefficient of thermal expansion and residual stresses in the specimens in Chapters 2 and 3.

Although four specimen types were used, this paper usually discusses only one specimen type in detail. Material properties used were taken from Chamis[4] with properties for +/- theta sets of helical plies being calculated with laminate theory using three dimensional considerations[5]. Table 1.2 shows the properties used in this thesis.

INNER LAMINATES

TENSION

PLY	THICKNESS	ANGLE FROM AXIAL	FIBER/MATRIX
1	0.01	0	SCRIM CLOTH
2	0.00746	90	S2 GLASS/EPOXY
3	0.00765	+20	"
4	0.00765	-20	"
5	0.00746	90	"
	0.04022		

COMPRESSION

(PLY #1 ABOVE THEN REPEAT PLIES 2-6 THREE TIMES)

OUTER LAMINATES

	TENSION	COMPRESSION		
1	0.00746	0.0224	90	S2 GLASS/EPOXY
2	0.00746	0.0224	+20	AS4 GRAPHITE/EPOXY
3	0.00746	0.0224	-20	"
4	0.00765	0.0229	+20	S2 GLASS/EPOXY
5	0.00765	0.0229	-20	"
6	0.00746	0.0224	90	"
	0.04514	0.1354		

Table 1.1 -- Cylindrical specimen configurations. Thicknesses in inches. Layers listed in order of inside to outside through thickness.

		CHAMIS	+/- 20° CHAMIS & HERAKOVICH
GRAPHITE/EPOXY			
E1	(psi)	20.600	13.082
E2	(psi)	1.193	1.220
E3	(psi)	1.193	1.225
ν_{12}		0.284	1.486
ν_{13}		0.284	-0.137
ν_{23}		0.334	0.293
G12	(psi)	0.602	2.632
G13	(psi)	0.602	0.472
G23	(psi)	0.446	7.576
α_1	(in/F)	0.06	--
α_2	(in/F)	18.06	(see Table 2.5)
α_3	(in/F)	18.06	--
GLASS/EPOXY			
E1		7.64	5.855
E2		1.95	1.857
E3		1.95	1.987
ν_{12}		0.284	0.566
ν_{13}		0.284	0.169
ν_{23}		0.387	0.342
G12		0.703	1.869
G13		0.703	2.504
G23		0.703	0.692
α_1		4.22	--
α_2		20.15	(see Table 2.5)
α_3		20.15	--

Table 1.2 -- Material properties determined using papers by Chamis and Herakovich.

CHAPTER 2 - COEFFICIENT OF THERMAL EXPANSION

2.1 Introduction

The temperature related experimental results were used to determine a coefficient of thermal expansion (CTE) for both the inner and outer compression specimens. These results were then compared to results obtained in closed form and finite element solutions and finally to results found in recent literature.

Key Figures:

Figures 2.5 and 2.6 present measured and corrected thermal expansion test data (heavy solid line), and the theoretical correlation (dashed line).

2.2 Experimental Results

2.2.1 Testing

Figures 2.1 and 2.2 show the actual readings taken from the test described on page 3 for the outer and inner specimens respectively. In Figure 2.1, the various symbols in the pre-75 degree range and those in the post-75 degree range represent different specimens. The same applies to Figure 2.2 for the whole range of temperatures, since only five inner specimens were tested in this manner (the repetition of symbols is due to a limitation of LOTUS 123 software). Keep in mind that the nonlinearity of these graphs should be

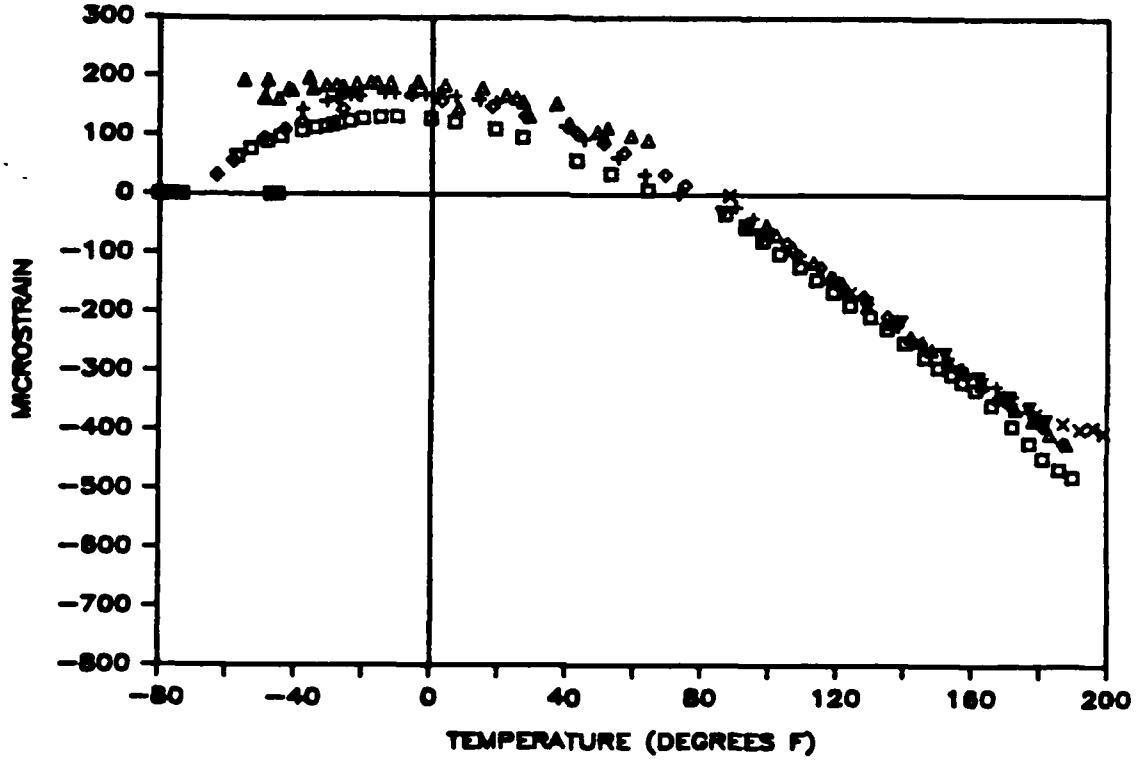

Figure 2.1 -- Axial Strain Gage Readings for Outers (p. 4).

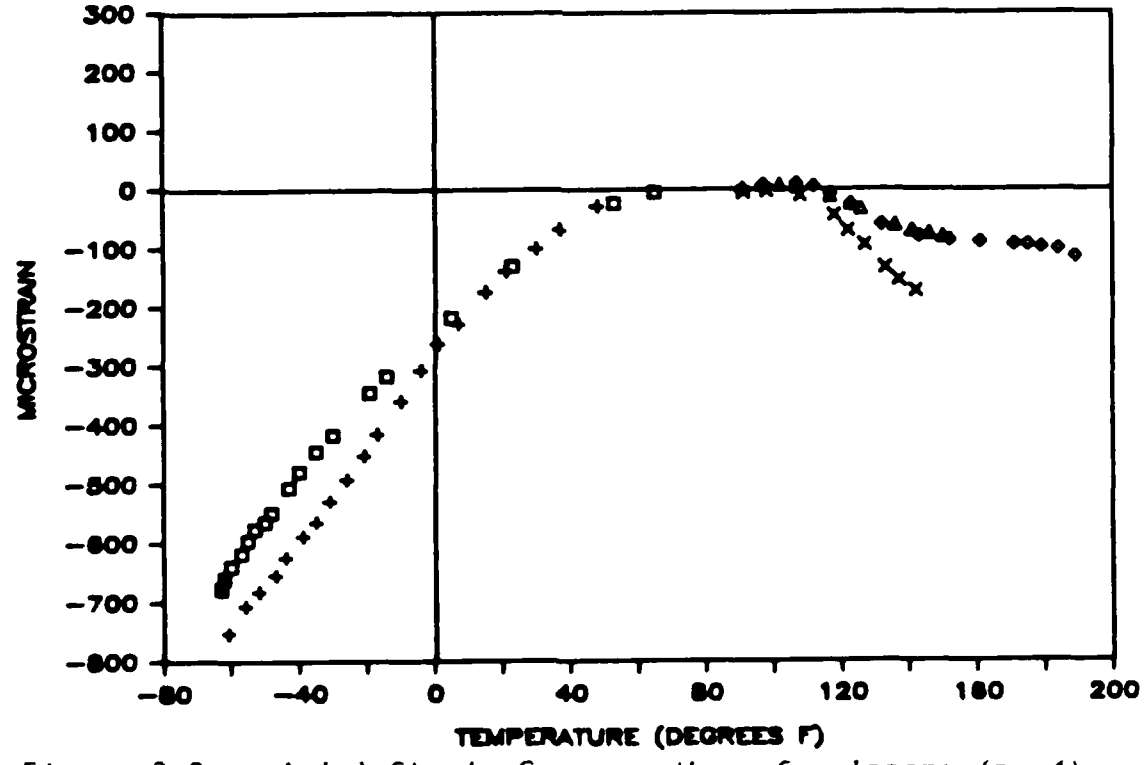

Figure 2.2 -- Axial Strain Gage readings for Inners (p. 4).

decreased by the superposition of compensation gage data.

Since there were no compensation gages used in the original testing, it was necessary to run additional compensation tests in order to determine the coefficient of thermal expansion. Preferably, one would use identical strain gages mounted on low-expansion National Bureau of Standards (NBS) standard reference material of fused silica concurrent with actual testing.[6,7,8] Also, it is desirable to heat the specimen in steps allowing thermal equilibrium between successive steps. This was not possible due to a prescribed temperature rate for the original tests of $5^{o}F$ per minute.

The gages used for compensation measurement were identical to those used on the original specimens (see the Appendix for gage information). Aluminum, a readily available material with a known linear coefficient of thermal expansion, was used. Two gages were mounted (one centered on each side) on a 2"x5"x1/8" 6061 T6 Aluminum specimen using the mounting methods described in Micro-Measurements Instructional Bulletins B-129-2[9] and B-127-9[10]. The IBM PC Portable, Measurements Group 2100 System Signal Conditioner and Amplifier, Metrabyte Dash-8 A/D Converter, DASHSOFT[3] program, and Omega 2168A digital thermocouple device described in Chapter I were used. The specimen was placed in a Precision Scientific Company 2700 watt oven (ranges from room temperature to $356^{o}F$). The temperature was increased at approximately five degrees Fahrenheit per minute as witnessed by the time vs. temperature graph of Figure 2.3 (approximately the same rate as the original testing). Figure 2.4 shows the temperature vs. strain

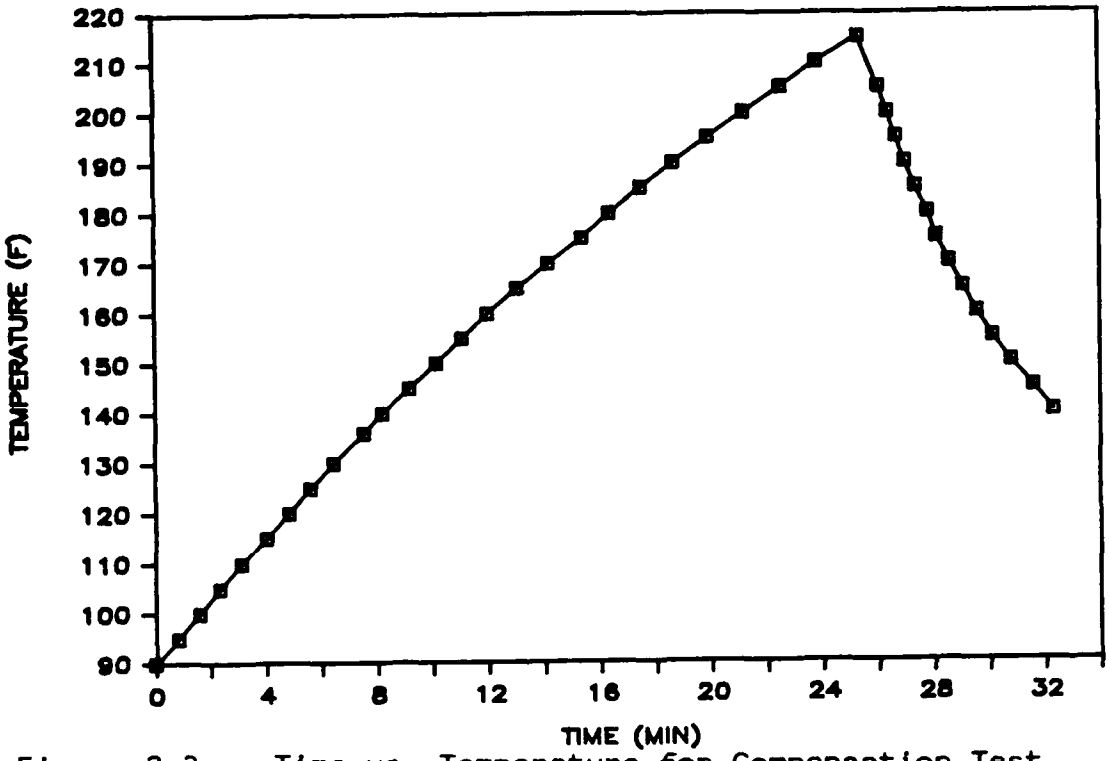

Figure 2.3 -- Time vs. Temperature for Compensation Test.

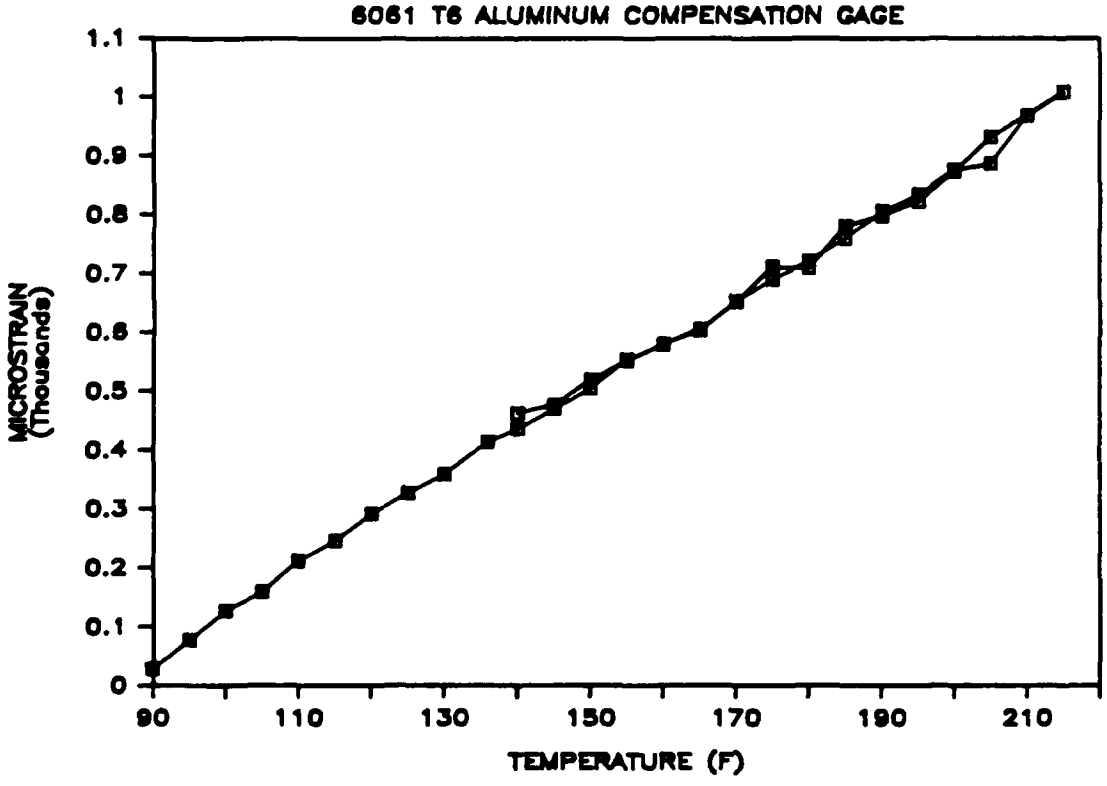

Figure 2.4 -- Temperature vs. Strain for Compensation Test.

for the compensation test . Note how the graph remains linear during "unloading."

2.2.2 Theory and Reduction of Data

A linear regression analysis[11] was then performed on this data to arrive at a linear coefficient of expansion due to both the gage and the aluminum specimen. To arrive at a CTE for the strain gage only, the methods described by Poore and Kesterson[6] and Measurements Group Tech Note 513[7] were used with slight modifications to allow for the fact that compensation gage testing was done after the original tests. We have,

$$CTE_{composite} = CTE_{measured} + CTE_{compensation}$$
$$= CTE_{measured} + (CTE_{aluminum} - CTE^{*})$$

where,

$CTE_{measured}$ = slope of strain-temperature graph for original composite specimens.
CTE^{*} = slope of strain-temperature graph for the aluminum compensation material.
$CTE_{aluminum}$ = the CTE known for 6061 T6 aluminum.

The slope of the strain-temperature graph for the aluminum alloy (Figure 2.4) was found to be 7.5 microstrain per degree F. Subtracting this from a "known" value for the CTE of the compensation material of 13.1 μ/F[22] we have $CTE_{compensation}$ = 5.6 μ/F. Tables 2.1 and 2.2 show, for the outer specimens, the measured CTE and the corrected CTE which represents the CTE of the composite cylinder in the axial and hoop directions respectively. Starred specimens are those with a coefficient of correlation greater than 0.998 calcu-

lated for $CTE_{measured}$. Values of CTE for highly non-linear data are measured on the first linear portion as the temperature drops below room temperature as indicated in Figure 2-1. The mean (AVE), standard deviation (SDEV), and coefficient of variation (COV) are calculated using only values from these starred specimens.

Referring back to Figure 2.1 for the outer specimens, the high temperature data is obviously fairly linear and linear coefficients of expansion were easily measured. However, the low-temperature specimens show a very non-linear relationship of strain with temperature. This non-linearity makes the determination of a linear CTE difficult as Table 2.2 shows a high coefficient of variation among the axial tubes. (The "hoop" direction gages are included in the tables. Their graphs are not shown for brevity, however. Although the plots were fairly linear, little can be concluded from one specimen in each temperature range.)

	SPECIMEN	DIRECTION	$CTE_{measured}$	$CTE_{composite}$
*	2-6-6	AXIAL	-3.96	1.64
*	2-4-3-3	AXIAL	-3.83	1.77
*	1-2-2-4	AXIAL	-4.14	1.46
*	1-1-3-3	AXIAL	-4.08	1.52
*	3-2-4-2	AXIAL	-3.69	1.91
*	3-4-3-2	AXIAL	-4.16	1.44
		AVE =	-3.98	1.62
		SDEV =	0.19	0.19
		COV =	0.05	0.12
*	2-6-6	HOOP	2.13	7.73

Table 2.1 -- Coefficients of Thermal Expansion for Hot-Dry Outer Specimens. All dimensional values are in $\mu/^{o}F$.

	SPECIMEN	DIRECTION	$CTE_{measured}$	$CTE_{composite}$
	3-4-3-3	AXIAL	-4.30	1.30
	3-4-4-2	AXIAL	-3.36	2.24
	3-4-5	AXIAL	-2.76	2.84
	3-4-6	AXIAL	-2.36	3.24
		AVE =	-3.19	2.41
		SDEV =	0.84	0.84
		COV =	0.26	0.35
*	3-4-6	HOOP	3.61	8.66

Table 2.2 -- Coefficients of Thermal Expansion for Low-Temperature Outer Specimens. All dimensional values are $\mu/^{o}F$.

Tables 2.3 and 2.4 show this information for the inner specimens in high-temperature and low-temperature tests respectively. The high non-linearity in the inner specimens occurred in the high-temperature range while the low-temperature range results are fairly linear as witnessed by Figure 2.2. As stated earlier, we expect the non-linearity of Figures 2.1 and 2.2 to decrease when we adjust them to include the effect of the compensation gage.

SPECIMEN	DIRECTION	$CTE_{measured}$	$CTE_{composite}$
1-2-1-1	AXIAL	-5.92	-0.32
3-3-4-2	AXIAL	-2.63	2.97
5-1-2-1	AXIAL	-3.46	2.14
	AVE =	-4.00	1.60
	SDEV =	1.71	1.71
	COV =	0.43	1.07
5-1-2-1	HOOP	(INCONCLUSIVE)	

Table 2.3 -- Coefficients of Thermal Expansion for Hot-Dry Inner Specimens. All dimensional values are in $\mu/^{o}F$.

SPECIMEN	DIRECTION	$CTE_{measured}$	$CTE_{composite}$
* 3-3-5	AXIAL	6.67	12.27
* 3-4-5	AXIAL	7.82	13.42
	AVE =	7.24	12.84
	SDEV =	0.81	0.81
	COV =	0.11	0.06
* 3-4-5	HOOP	7.84	13.44

Table 2.4 -- Coefficients of Thermal Expansion for Low-Temperature Inner Specimens. All dimensional values are $\mu in/^{o}F$.

The equation for the linearized form of Figure 2.4 is STRAIN=5.6*TEMPERATURE-464. If, instead of measuring the CTE of the specimens before adding the effect of the compensation gage, this equation is superimposed onto Figures 2.1 and 2.2; the non-linearity can be reduced and the actual CTE of the material can be measured directly. Consequently, Figures 2.5 and 2.6 are simply this superposition. They indicate the actual strain of the cylinders under change in temperature. The data points still indicate a significant non-linearity despite an obvious reduction from Figures 2.1 and 2.2. This non-linearity represents a problem in determining a single linear coefficient of thermal expansion for the test materials. The solid curved lines in Figures 2.5 and 2.6 indicate a cubic spline analysis using five-point smoothing[11]. Both curves have coefficients of correlation greater than 0.9990. The dashed lines in Figures 2.5 and 2.6 represent the data predicted by the closed form and finite element solutions in Sections 2.3 and 2.4. Finally, the heavy solid line indicates the pre-

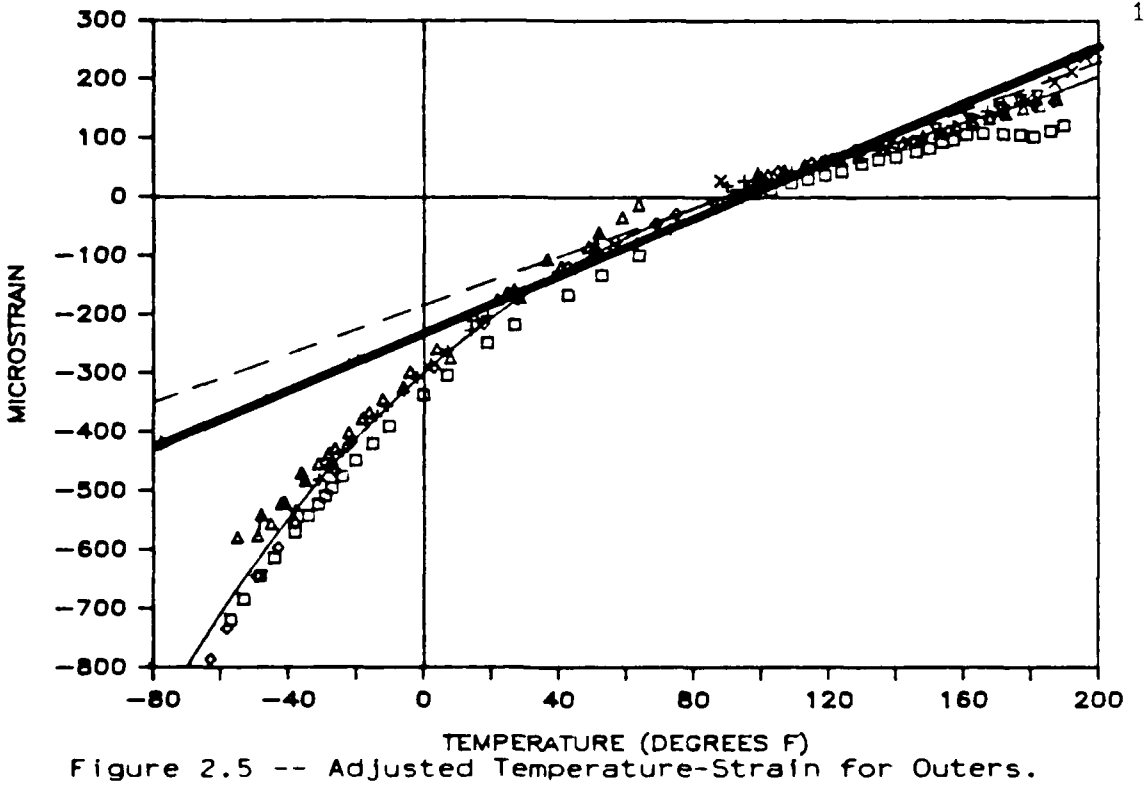

Figure 2.5 -- Adjusted Temperature-Strain for Outers.

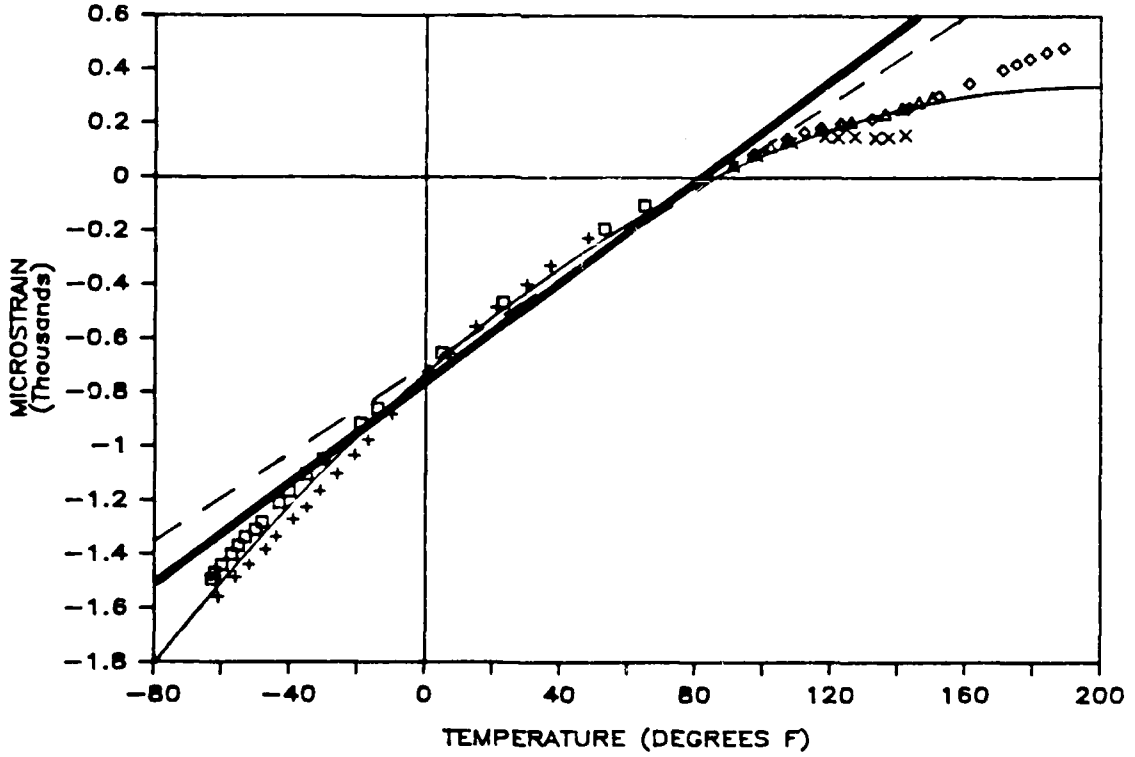

Figure 2.6 -- Adjusted Temperature-Strain for Inners.

dicted thermal expansion after compensation adjustments discussed in the following paragraphs.

2.2.3 Compensation Adjustment

The non-linearity of both inners and outers is consistent among the data available. One possibility may be that the compensation measurement is not accurate enough. A decrease in the compensation value (5.6 $\mu/^{o}F$) would decrease the amount of reduction in non-linearity while an increase in the compensation would decrease the non-linearity of the final material strain-temperature curve.

Therefore, if $CTE_{compensation}$ were, say, 5.7 $\mu/^{o}F$, the curve of Figures 2.5 and 2.6 would be more linear, thus decreasing the change in CTE with change in temperature. Since a value of CTE for aluminum of 13.1 $\mu/^{o}F$ was used, an error of only 0.75% in this value can significantly change the data. This is why it is preferable to use a compensation material with a very low coefficient of expansion, such as the fused silica mentioned earlier. If $CTE_{compensation}$ is increased until Figures 2.5 and 2.6 become nearly linear over a range not including the extreme ends (using LOTUS 123), we arrive at $CTE_{compensation}$=5.67 and a linear coefficient of expansion of the test material of 9.72 $\mu/^{o}F$ and 2.63 $\mu/^{o}F$ for the inner and outer specimens respectively (see Table 2.9 on page 28 for compared results). This corresponds to a CTE for 6061 T6 Aluminum of 13.17 $\mu/^{o}F$ compared to the original assumed value of 13.10 $\mu/^{o}F$ from Military Handbook 17[22]. This value was consistent for both inner and outer specimens.

2.3 Closed Form Solution

2.3.1 TDCYL2 Program

Closed form solutions were found for inner and outer, tension and compression specimens using the FORTRAN program TDCYL2 written by N.L. Newhouse[25]. TDCYL2 uses a closed form method to calculate the stresses and strains in the three principal directions at any radial position through the thickness of a composite cylinder. TDCYL2 accepts material properties only in the meridional, hoop, and radial directions (m,h,r) as shown in Figure 2.7.

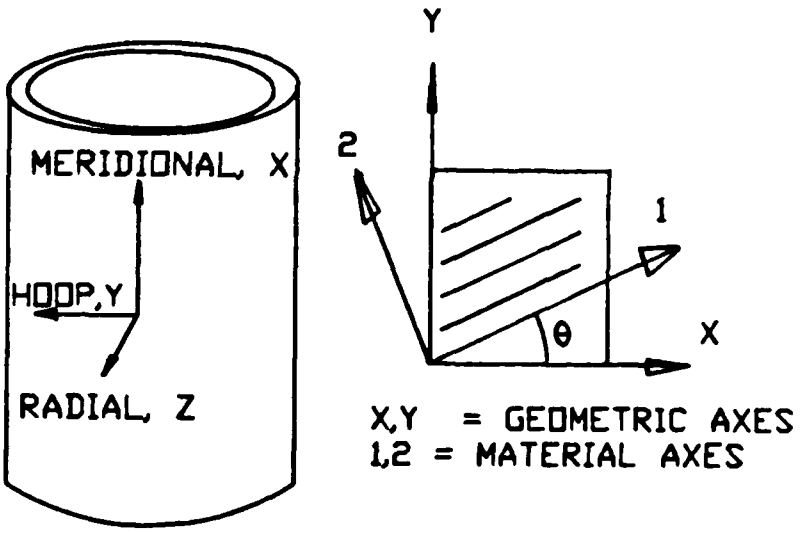

Figure 2.7 -- Coordinate systems.

Therefore, in order to use TDCYL2 in the determination of thermal strains, coefficients of thermal expansion must be input for each layer in the meridional, hoop, and radial directions. As outlined in Table 1.2 the Chamis[4] properties for CTE were used, namely,

S-GLASS/EPOXY	AS-4 GRAPHITE/EPOXY
α_1=4.22 μ/°F	α_1=0.06 μ/°F
α_2=20.15 "	α_2=18.06 "
α_3=20.15 "	α_3=18.06 "

2.3.2 Determination of Helical Ply Coefficients

Now, for the transformation of CTE from the 1,2 coordinate to the m,h coordinate, we have,

$$\begin{bmatrix} \alpha_m \Delta T \\ \alpha_h \Delta T \\ \alpha_{mh} \Delta T \end{bmatrix} = \begin{bmatrix} m^2 & n^2 & 2mn \\ n^2 & m^2 & -2mn \\ -mn & mn & m^2-n^2 \end{bmatrix} \begin{bmatrix} \alpha_1 \Delta T \\ \alpha_2 \Delta T \\ \alpha_{12} \Delta T = 0 \end{bmatrix} \qquad (2\text{-}1)$$

where $m=\cos(\theta)$ and $n=\sin(\theta)$. This reduces to,

$$\alpha_m = \alpha_1 \cos^2\theta + \alpha_2 \sin^2\theta \qquad (2\text{-}2)$$

$$\alpha_h = \alpha_1 \sin^2\theta + \alpha_2 \cos^2\theta \qquad (2\text{-}3)$$

$$\alpha_{mh} = -\alpha_1 \cos\theta \sin\theta + \alpha_2 \cos\theta \sin\theta \qquad (2\text{-}4)$$

As long as we are dealing with 0 and 90 degree plies we can use equations (2-2) through (2-4) since (2-4) becomes zero (TDCYL2 does not accept α_{mh} as input). However, since we have +/- 20 plies we must find a way to cancel out α_{mh}. This can be done by including a $+\theta$ ply along with a $-\theta$ ply as a single layer in an analysis using lamination theory.

The problem, then, is to find α_m, α_h, α_r for a +/- theta laminate given α_1, α_2, α_3 and the stiffness properties of the individual plies. For this analysis, let the coordinate sys-

tem x,y,z be congruent to m,h,r. From general laminate theory we have equations (2-5), (2-6), and (2-7); where [T] is the two-dimensional transformation matrix, $[T]^{-1}$ is its inverse, $[Q_{ij}]_k$ is the stiffness matrix for the kth layer, $[\sigma_{x,y}]_k$ is the stress vector for the kth layer, and $[\epsilon_{x,y}]_k$ is the strain vector for the kth layer.

$$[T] = \begin{bmatrix} m^2 & n^2 & 2mn \\ n^2 & m^2 & -2mn \\ -mn & mn & m^2-n^2 \end{bmatrix} \tag{2-5}$$

$$[T]^{-1} = \begin{bmatrix} m^2 & n^2 & -2mn \\ n^2 & m^2 & 2mn \\ mn & -mn & m^2-n^2 \end{bmatrix} \tag{2-6}$$

$$[\sigma_{x,y}]_k = [T]^{-1}[Q_{ij}]_k[T][\epsilon_{x,y}]_k \tag{2-7}$$

We then define $[\bar{Q}_{ij}]_k$ as the matrix multiplications $[T]^{-1}[Q_{ij}]_k[T]$ and equation (2-7), with the thermal expansion terms added in, becomes,

$$\begin{bmatrix} \sigma_x \\ \sigma_y \\ \sigma_{xy} \end{bmatrix}_k = \begin{bmatrix} \bar{Q}_{11} & \bar{Q}_{12} & 2\bar{Q}_{16} \\ \bar{Q}_{12} & \bar{Q}_{22} & 2\bar{Q}_{26} \\ \bar{Q}_{16} & \bar{Q}_{26} & 2\bar{Q}_{66} \end{bmatrix}_k \begin{bmatrix} \epsilon_x - \alpha_x\Delta T \\ \epsilon_y - \alpha_y\Delta T \\ \epsilon_{xy} - \alpha_{xy}\Delta T/2 \end{bmatrix} \tag{2-8}$$

For the thickness, t_k, distance to midlayer from reference, z_k, and the $\bar{Q}$ matrix of each layer we can define,

$$A_{ij} = \sum_{k=1}^{n} (\bar{Q}_{ij})_k t_k \qquad (2\text{-}9)$$

$$B_{ij} = \sum_{k=1}^{n} (\bar{Q}_{ij})_k t_k z_k \qquad (2\text{-}10)$$

where n is the number of layers and A_{ij} and B_{ij} are matrices coupling midlayer strain, ϵ_o, and curvature, k, to the running load, N_{ij}.

$$[N] = [A][\epsilon_o] + [B][k] - [N]^T \qquad (2\text{-}11)$$

where $[N]^T$ is the running thermal load.

$$[N_{ij}]^T = \sum_{k=1}^{n} \int_{h_{k-1}}^{h_k} (\bar{Q}_{ij})_k (\alpha_{ij})_k \Delta T dz \qquad \text{for } i,j=1,2,6 \qquad (2\text{-}12)$$

We can evaluate the integral as follows:

$$\int_{h_{k-1}}^{h_k} \bar{Q}_{ij} \alpha_{ij} \Delta T dz = \bar{Q}_{ij} \alpha_{ij} \Delta T (h_k - h_{k-1})$$

$$= \bar{Q}_{ij} \alpha_{ij} \Delta T t \qquad (2\text{-}13)$$

Therefore,

$$[N_{ij}]^T = \sum_{k=1}^{n} (\bar{Q}_{ij})_k (\alpha_{ij})_k \Delta T t_k$$

$$= \Delta T \sum_{k=1}^{n} (\bar{Q}_{ij})_k (\alpha_{ij})_k t_k \qquad (2\text{-}14)$$

From equation (2-11) we assume there is no curvature so [B] = 0. Therefore we can say,

$$[N] = [A][\epsilon_o] - [N]^T \qquad (2\text{-}15)$$

Since we are applying only a change in temperature, we can say [N]=0 and it follows that,

$$[A][\epsilon_o] = [N]^T \qquad (2\text{-}16)$$

Now premultiply by $[A]^{-1}$,

$$[\epsilon_o] = [A]^{-1}[N]^T \qquad (2\text{-}17)$$

Now, replacing $[N]^T$ in equation (2-17) by equation (2-14) and writing in $[\epsilon_o]$,

$$\begin{Bmatrix} \alpha_x \\ \alpha_y \\ \frac{\alpha_{xy}}{2} \end{Bmatrix}_{\pm\theta} = [A]^{-1} \left\{ \Delta T \sum_{k=1}^{n} (\bar{Q}_{ij})_k (\alpha_{ij})_k t_k \right\} \qquad (2\text{-}18)$$

$$i,j = 1,2,6$$

where $(\alpha_{ij})_\theta = (\alpha)_{x,y}$ for a theta degree ply.

The $\bar{Q}_{ij}$ terms are easily computed and, hence, the A_{ij} and $[A]^{-1}$ terms (a programmable calculator was used for the 3x3 operation. A Gaussian Elimination[11] procedure was used to invert the A matrix). Now, assuming ΔT=1 degree F and inputting the original values for CTE in the 1,2 directions from Chamis[4], CTE's for the x,y (m,h) coordinate system can be computed. The -xy or -mh terms drop out for +/-theta laminates. Table 2.5 shows the results for our two materials in +/- 20 degree configurations. Since this theory applies only to the x,y (m,h) coordinates, the radial CTE is assumed to be equal to the hoop CTE as would be expected.

	AS4-Graphite/Epoxy	S2-Glass/Epoxy
α_x	-1.6×10^{-6}/F	3.4×10^{-6}/F
α_y	14.3×10^{-6}/F	19.0×10^{-6}/F
α_z	14.3×10^{-6}/F	19.0×10^{-6}/F

Table 2.5 -- Calculated values for CTE for a +/- 20° layer using laminate theory.

A two-dimensional analysis using general laminate theory on individual plies in the program MATL[21] yields the results of Table 2.6.

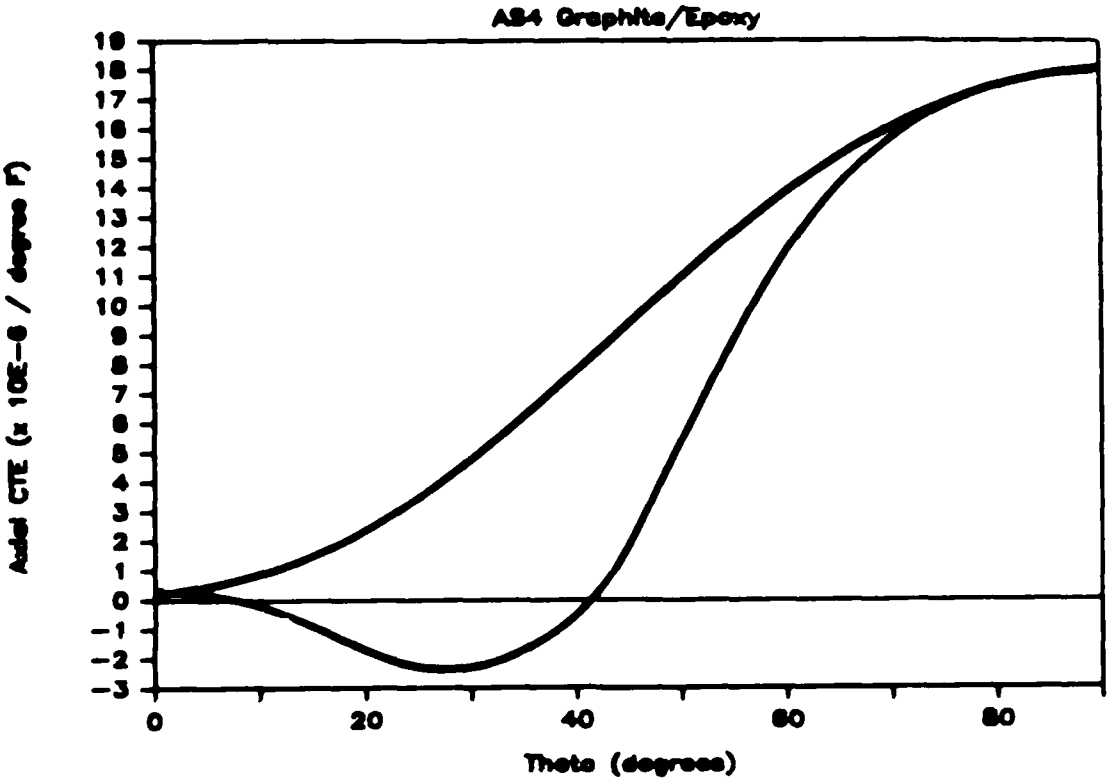

Figure 2.8 -- CTE vs. Ply Orientation Angle.

	AS4-Graphite/Epoxy	S2-Glass/Epoxy
x	-1.57×10^{-6}/F	3.40×10^{-6}/F
y	15.35×10^{-6}/F	18.74×10^{-6}/F
z	15.35×10^{-6}/F	18.74×10^{-6}/F

Table 2.6 -- Calculated values for CTE for +/- 20 degree laminate using two-dimensional single ply solution.

Using the above method, CTE can be plotted against different values of theta for both a single theta ply and a +/- theta laminate as shown in Figure 2.8. Herakovich[5] discusses this phenomena with respect to other material properties with emphasis on negative through-the-thickness Poisson's ratios.

2.3.3 TDCYL2 Results

These properties of CTE and the Chamis[4] material properties of Table 1.2 were then entered into TDCYL2 with the results shown in Table 2.7 for tension and compression, and inner and outer specimens. (Radial CTE's for graphite and glass helicals used were 19.3 μ/°F and 20.8 μ/°F due to earlier predictions of CTE).

	TENSION		COMPRESSION	
	INNER	OUTER	INNER	OUTER
α_x	8.07 μ/F	2.38 μ/F	8.89 μ/F	2.41 μ/F
α_y	7.26	8.73	7.50	9.16

Table 2.7 -- TDCYL2 Coefficient of Thermal Expansion output.

Only compression specimen CTE results can be compared with experimental results since only compression members were tested for CTE. Referring back to Table 2.2 we see that the outer low-temp specimens compare very well but in Table 2.4 the closed form solution falls short of the measured value. Remember, however, the problem of non-linearity. The values for CTE after incrementing $CTE_{compensation}$ in Section 2.2 are very close to those predicted by TDCYL2 in Table 2.7 with a coefficients of variation of 6.3% and 6.2% for the inner and outer laminates, respectively (for comparison, see Table 2.9 on page 28).

2.4 Finite Element Solution

2.4.1 Description of ANSYS

For a finite element solution, the proprietary program ANSYS, version 4.2, available on the UNL VAX system was used. ANSYS is a software engineering analysis system produced and sold by Swanson Analysis Systems, Inc., Houston, Pennsylvania. ANSYS capabilities include structural analysis (static and dynamic; elastic, plastic, creep, and swelling; buckling; small and large deflection theory), heat transfer analysis (steady-state and transient; conduction, convection, and radiation; phase change), uncoupled thermal-stress analysis (temperatures from a heat transfer analysis available for input into a Structural analysis), coupled thermal stress, and electromagnetic field analysis. ANSYS was originally designed (1970) from the ground up mainly for isotropic materials. Capabilities to handle anisotropic and non-linear materials were added later. The use of ANSYS in the investigation of composites appears to be a rarely attempted endeavor and its inclusion in this paper serves not only as a finite element tool to compare with other solutions but also as a study of this general purpose program's applicability to research in composite materials characterization.

2.4.2 ANSYS Input

Figure 2.9 is the ANSYS input data for the thermal analysis of the outer-tension specimens (Data for the other specimen configurations is not included for brevity). The "NL"

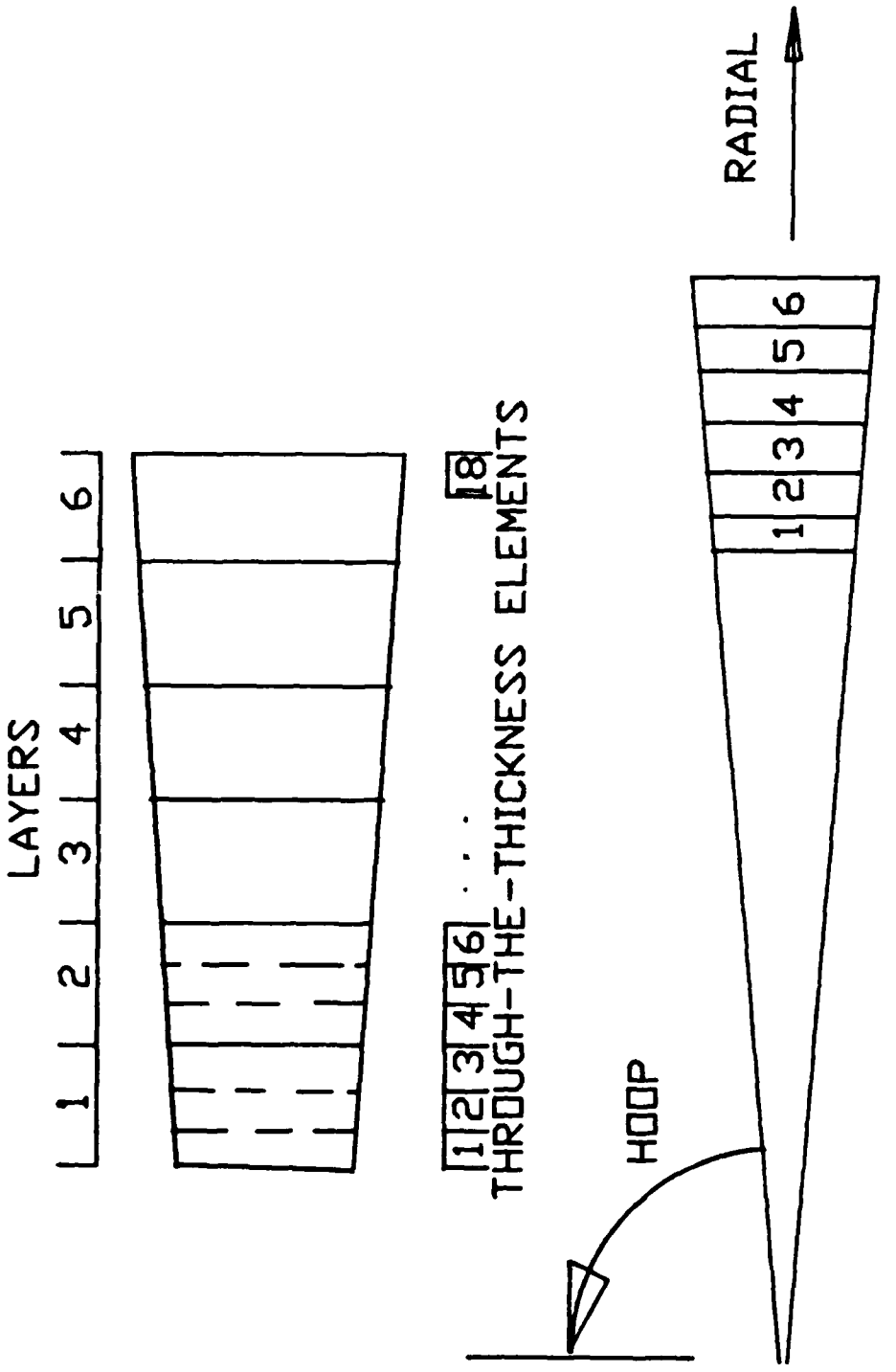

Figure 2.9 -- Finite Element Model used in ANSYS.

commands give the material properties in the form of a 6x6 stiffness matrix equivalent to the Q matrix discussed earlier. The "N" and "E" commands define the nodes and elements respectively. Figure 2.10 shows the element configuration used to model the composite cylinder for thermal analysis. Scale is exaggerated to show how the elements define a cylindrical shell. In the model, each layer of composite is characterized by three to five elements in a

```
/PREP7//TITLE,TENSION,OUTER,INTERLAMINAR,OUT-
TEMP.DAT,TEMPERATURE RUN
ET,1,64,0,0,0,0,0,0
NL,1,1,2.408E6/NL,1,7,0.968E6/NL,1,13,1.002E6/NL,1,37,8-
.190E6 NL,1,43,0.968E6/NL,1,67,2.408E6/NL,1,91,0.703E6
NL,1,109,0.703E6/NL,1,121,0.703E6/NL,6,1,2.408E6
NL,6,7,0.998E6/NL,6,13,0.972E6/NL,6,37,2.480E6
NL,6,43,1.573E6/NL,6,67,6.910E6/NL,6,91,0.692E6
NL,6,109,1.869E6/NL,6,121,..504E6/NL,7,1,1.356E6
NL,7,7,0.468E6/NL,7,13,0.51E6/NL,7,37,1.698E6/NL,7,43,2-
NL,7,67,16.665E6/NL,7,91,0.472E6/NL,7,109,2.632E6
NL,7,121,7.576E6/ALPX,1,20.15E-6/ALPY,1,4.22E-6
ALPZ,1,20.15E-6/ALPX,6,20.80E-6/ALPY,6,19.01E-6
ALPZ,6,3.36E-6/ALPX,7,19.356E-6/ALPY,7,14.254E-6
ALPZ,7,-1.621E-6/CSYS,1
N,1,1.390/N,5,1.392487/N,9,1.394974
N,13,1.39746/N,17,1.399947/N,21,1.402434/N,25,1.40492
N,29,1.407404/N,33,1.409894/N,37,1.41238/N,41,1.41493
N,45,1.41748/N,49,1.42003/N,53,1.42258/N,57,1.42513
N,61,1.42768/N,65,1.430167/N,69,1.432654/N,73,1.43514
NGEN,2,1,1,73,4,0,0,.002/NGEN,2,2,1,74,1,0,0.125,0
NROTAT,1,76,1/MAT,1/E,1,2,4,3,5,6,8,7
E,5,6,8,7,9,10,12,11/E,9,10,12,11,13,14,16,15/MAT,7
E,13,14,16,15,17,18,20,19/E,17,18,20,19,21,22,24,23
E,21,22,24,23,25,26,28,27/E,25,26,28,27,29,30,32,31
E,29,30,32,31,33,34,36,35/E,33,34,36,35,37,38,40,39/MAT-
,6 E,37,38,40,39,41,42,44,43/E,41,42,44,43,45,46,48,47
E,45,46,48,47,49,50,52,51/E,49,50,52,51,53,54,56,55
E,53,54,56,55,57,58,60,59/E,57,58,60,59,61,62,64,63/MAT-
,1 E,61,62,64,63,65,66,68,67/E,65,66,68,67,69,70,72,71
E,69,70,72,71,73,74,76,75/CPSIZE,40 CP,1,UX,1,3/CP,2,UX
,2,4/CP,3,UX,73,75/CP,4,UX,74,76/CPNGEN,5,UZ,2,76,2
CPNGEN,6,UY,1,73,4/CPNGEN,7,UY,2,74,4/ITER,-5,5
D,3,UY,0.,,75,4/D,4,UY,0.,,76,4/D,1,UZ,0.,,75,2/TREF,10 -
0 KTEMP,0/TUNIF,0/AFWRITE/FINISH//INPUT,27/FINISH
```

Figure 2.10 -- ANSYS input data for thermal analysis.

through-the-thickness manner. This "stack" of layers is then rotated about the z, or axial, axis to form a ring which, with the proper boundary conditions, represents the

"test section" of a test cylinder. This model works well in representing a long cylinder under thermal or tensile loads (A buckling analysis requires a model which includes the entire length of the cylinder which loses the three-dimensional capabilities of the present model.). The "CP" and "D" commands define the coupled degrees of freedom and the boundary conditions respectively. Finally, "TREF" and "TUNIF" define the initial reference temperature and the applied uniform temperature.

Since the material properties input is in the form of the Q matrix, this must be calculated separately. Coefficients of thermal expansion for the individual plies must also be calculated and input for the axial, hoop, and radial directions thus requiring the same calculations used in TDCYL2.

The stress results from TDCYL2 and ANSYS will be discussed in Chapter 3, Residual Stresses. CTE results from

	TENSION		COMPRESSION	
	INNER	OUTER	INNER	OUTER
axial	8.074 μ/F	2.376 μ/F	8.887 μ/F	2.408 μ/F
hoop	7.260	8.732	7.503	9.156

Table 2.8 -- ANSYS Coefficient of Thermal Expansion output.

ANSYS are shown in Table 2.8. The results are essentially the same as for the three-dimensional closed form solution using TDCYL2 (Table 2.7). The similarity of these results

provides some insight into the applicability of ANSYS to composite materials and, specifically to thermal modeling of cylindrical laminates.

2.5 Literature Results

The comparison of exact results for our particular laminates is certainly not possible due to the uniqueness of the layering variables. This is often, if not always, a problem in the study of applicable composite laminates. The variety of possible fiber and matrix materials and their countless configurations is so great that the classical comparison of empirical data used in the study of metals is an impossible task. We often rely on trends, general observations, or possibly models developed from data resulting from various configurations of like materials.

Freeman and Campbell[15] studied the thermal expansion of various graphite reinforced composites under temperatures ranging from -300°F to 500°F. They obtained results similar to Figure 2.8 experimentally thus indicating the variability of CTE with various ply orientations. They also reported CTE's at three different ranges of temperature; -320 to 75°F, 75 to 350°F, and -320 to 350°F. CTE's sometimes tripled from the first to the second range for particular graphite composites. This change is not as dramatic for graphite composites considering their small CTE but could be a more important consideration for laminates with higher CTE's (ie. tripling a CTE=0.7 compared to tripling a CTE=4 μ/°F). Freeman and Campbell reported an increase in CTE with increases in tem-

perature.

Daniel[16] also reports significant increases in thermal expansion coefficients with increases in temperature for graphite/epoxy and S-glass/epoxy unidirectional composites. However, for some laminates with both 0 and +/- 45 plies the CTE actually decreased with increasing temperatures. Sufficient data was not available to make any general conclusions about laminate configuration and change in CTE with temperature. This appears to be a possible subject for further investigation.

2.6 Conclusions

Table 2.9 indicates test and theory coefficients of thermal expansion as presented in this chapter. A conclusion is that linear coefficients of thermal expansion for filament wound laminates can be predicted using classical laminate theory.

LINEAR COEFFICIENTS OF THERMAL EXPANSION for COMPRESSION SPECIMENS (microstrain/^{o}F)

	TEST		THEORY	
	OUTER	INNER	OUTER	INNER
x	2.63	9.72	2.41	8.89
y	(INSUFFICIENT DATA)		9.16	7.50

Table 2.9 -- Comparison of Test vs. Theory for Linear Coefficients of Thermal Expansion for Compression Specimens.

CHAPTER 3 - RESIDUAL STRESSES

3.1 Background

Residual stresses are a function of many parameters, such as type of fiber and matrix, fiber volume ratio, ply orientation, curing temperature and other variables. They can reach values comparable to the transverse strength of the ply and thus induce cracking of that ply within the laminate. They reach equilibrium with interlaminar shear stresses transmitted from adjacent plies and can thus cause delamination. In the design and evaluation of composite structures one must take residual stresses into account and superimpose them onto those produced by subsequent external loading.

Residual stresses are often called "fabrication stresses" since they result from the fabrication process. An important factor of this process is the cure cycle. From the cure cycle we can determine a change in temperature from maximum cure temperature to test temperature. For both inner and outer specimens, the maximum cure temperature was 275 +/-10^{o}F and the typical test temperature was 72 +/- 5^{o}F. This yields a change in temperature of 188 to 218^{o}F. Using this change in temperature we can approximate the inherent residual stresses at the time of testing. These residual stresses can then be superimposed upon the actual test results to yield a more accurate picture of the actual stresses at failure.

As in Chapter 2, experimental results are compared to

closed form and finite element solutions. Results from the TDCYL2 and ANSYS programs will be discussed first, followed by a simple test procedure to determine residual stresses in cylindrical composites.

Key Figure:

Figure 3.1.b shows the hoop residual stresses as predicted by TDCYL2 and ANSYS as the solid line. The dashed line represents those residual stresses predicted by the bench test discussed in Section 3.3.

3.2 Closed Form and Finite Element Solutions

These solutions are discussed simultaneously since the methods were covered in Chapter 2 and the results from each solution are very similar. Using an average ΔT of $203^{\circ}F$ $+/-15^{\circ}F$, Tables 3.1 and 3.2 are the results obtained from TDCYL2 and ANSYS respectively for the outermost fibers only. Using only temperature effects, these results are our best analytical prediction of residual stresses. Since the stresses in Tables 3.1 and 3.2 are for the radially-outermost fibers, the radial stress is a stress normal to the surface which is equal to zero. Although residual stress calculations were performed on all four types of specimens, only complete results for the outer tension specimens will be shown for brevity.

The three graphs of Figure 3.1 show the distribution of radial, hoop, and axial stresses through the thickness of the specimen. Tensile radial stresses, which would add to a delaminating critical stress, are highest between the glass

STRESS (psi)	TENSION		COMPRESSION	
	INNER	OUTER	INNER	OUTER
σ_x	4535	6666	4174	6602
σ_y	-3421	-5095	-3910	-5792
σ_z	0	0	0	0

Table 3.1 -- TDCYL2 output for T=-203 F. All values are in psi.

STRESS (psi)	TENSION		COMPRESSION	
	INNER	OUTER	INNER	OUTER
σ_x	4529	6662	4182	6610
σ_y	-3418	-5094	-3911	-5797
σ_z	0	0	0	0

Table 3.2 -- ANSYS output for ΔT=-203 F. All values are in psi.

helicals and the glass hoops, yet are very low compared to failure allowables discussed in Chapter 4. The hoop and axial residual stresses are more significant. The only tensile hoop stress is 4.65 ksi in the glass helical layer. A value of 4.37 ksi of this stress acts in a transverse direction to the glass fibers. This contributes considerably to an assumed failure stress[23] of 7 ksi for S-glass/Epoxy in transverse tension. More significantly, the axial residual stress in the glass hoop layers is as high as 6.69 ksi in tension. This is very near a failure stress and we might expect some matrix cracking in the specimens after cure or

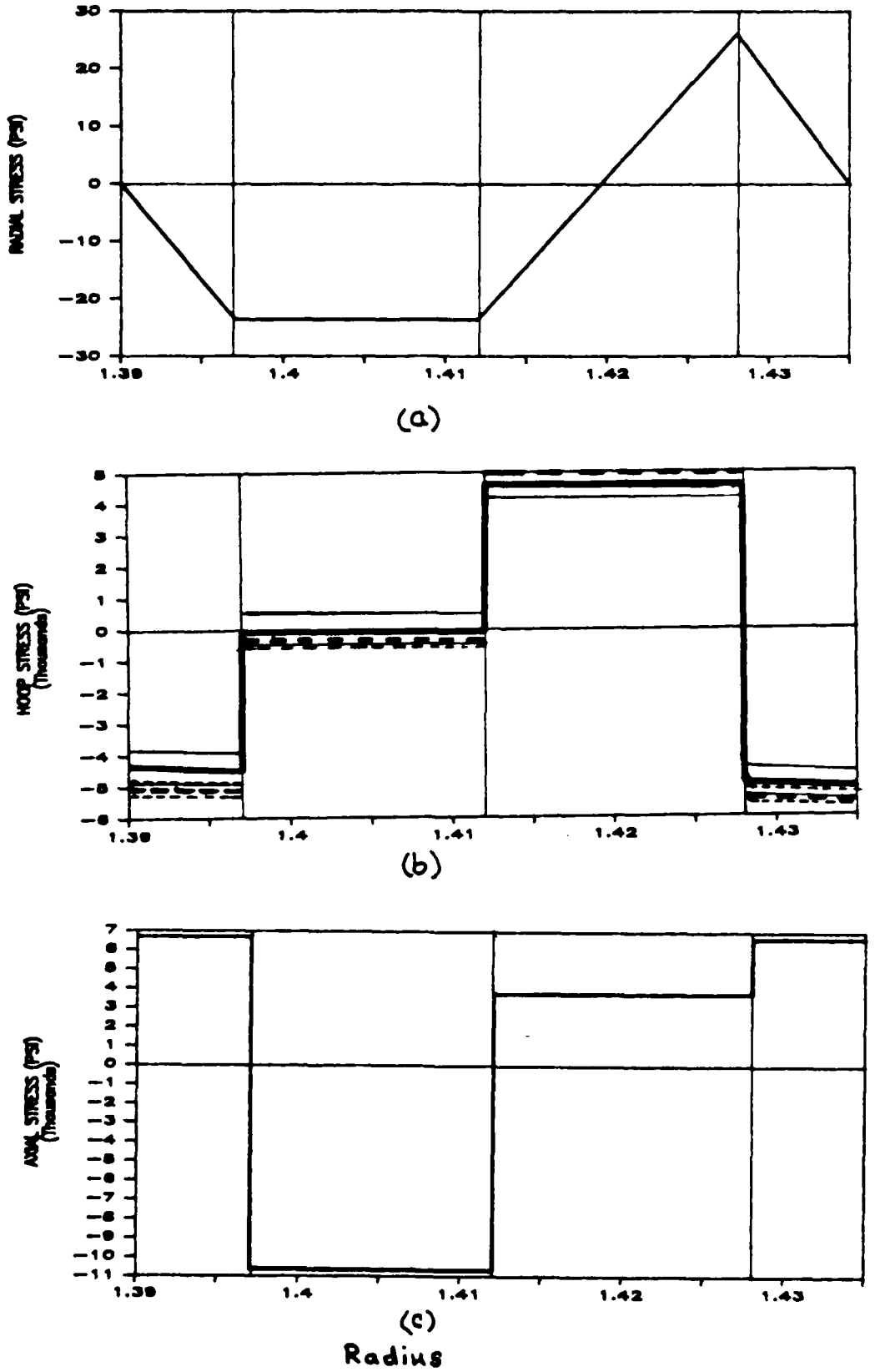

Figure 3.1 -- ANSYS Residual Stresses for Outer Tension Spec.

under small load conditions.

Since there appeared to be no cracking of the matrix in any of the specimens prior to testing, these residual stresses may be a high prediction or the allowable may be low. This shows the need, not only for testing of allowables, but also for tests to measure residual stresses. The following section will investigate a method to measure residual stresses in composite tubes. Testing of allowables will be discussed in Chapter 4.

3.3 Residual Stress Bench Test

Voyiadjis et.al.[26] measured residual stresses in composite cylinders by removing material from the inner and outer surfaces and measuring the resulting strain on the opposite surface. This same idea can be used more simply by relieving the stress and measuring a change in radius instead of a change in length. By measuring the change in inner radius upon relief of the residual stresses in the hoop direction, these stresses can be calculated. The only unknown is the change in inner radius.

To produce more specimens and make cutting of specimens easier, 3/4", 1", and 1 1/4" rings were cut from an outer tension cylinder which had not been previously tested. The inner surface was used for measurements because of its smooth surface due to its fabrication on a mandrell. The inside diameter was measured using inside calipers which were then measured using an outside micrometer. This being recorded, the ring specimens were cut once at 90 degrees

off the recorded diameter. This cut relieved the hoop residual stress in the specimen and another measurement of inner diameter was taken at the same points of measurement as before.

For six tests, two for each width of specimen, the average initial radius, R_o, and average final radius, R_f, were 1.390 +/-0.002 inches and 1.3680 +/- .002 inches respectively. This corresponds to a change in radius of -0.022 +/- 0.002 inches. The coefficients of variation were 0.36% and 0.58% respectively. There was no relation between width and change in radius. (The indication of error in the readings is necessary since a relatively small error results in fairly large changes in final stresses.)

The change in curvature can be computed as follows,

$$\Delta K = (1/R_o - 1/R_f) = 1/1.390 - 1/1.368 = -0.0116 +/- 0.0021$$

This change in curvature can then be input to MATL[21] to get the moment, M_{test}.

$$M_{test} = -0.526 +/- 0.095 \quad \text{in-lb/in}$$

Now this is compared to the moment calculated from the ANSYS and TDCYL2 results for hoop stress in Figure 3.1.b.

$$M_{predicted} = -0.438 +/- 0.033$$

The measured residual stresses can be calculated by multiplying the values in Figure 3.1 by 0.526/0.438 = 1.20. In Figure 3.1.b, the heavy solid line is the values predicted by ANSYS, the thinner solid lines are the error due to error in cure temperature, the heavy dashed line is the values predicted by the bench test, and the thinner dashed lines are the error in that measurement due to micrometer reading

errors.

3.4 Conclusions

The overlapping of the ranges in Figure 3.1 indicates a good ability to predict residual stresses using TDCYL2 and ANSYS. One shortcoming is that both computer solutions and measurements of the change in radius rely on accurate determination of the coefficients of thermal expansion and other material properties.

It has been shown that radial residual stresses do not add to the tensile interlaminar normal stresses in the region where delamination occurred in the original test specimens (see p. 3), but actually decrease them slightly.

Fairly significant residual stresses have been shown in the transverse direction in glass hoop and helical plies, possibly resulting in matrix cracking during cool down from cure.

CHAPTER 4 - DELAMINATION ALLOWABLES

4.1 Introduction

Foral and Gilbreath's[2] continuing research in modes of failure in composite materials indicates, along with current literature[17,18,19,20], a growing concern about delamination failures. The modes of failure in filament wound composites are particularly complex. Both predicting the type and sequence of failures and analyzing the actual failures which took place in a closely observed loading are difficult yet necessary for the characterization of the material.

The purpose of this chapter is to investigate finite element solutions compared to closed form solutions of the three-dimensional state of stress in a filament wound composite cylinder under axial tension. Those interlaminar stresses contributing specifically to delamination failures will be discussed. A discussion of the problem of discontinuities at the ends of the cylindrical test specimen caused by static test grips in relation to delamination causing stresses is included. Finally, experimental determination of the allowables which govern the stresses at which delamination failures occur will be attempted.

In his programs TUBE and TDCYP, Gilbreath[3] analyzes the three-dimensional state of stress in the test section of the tubular specimen (that section of the cylinder not affected by the discontinuities at the ends). Gilbreath uses the "exact"

method developed by Waltz and Vinson[27]. The method involves five differential equations for each distinct layer in a composite cylinder. Gilbreath's solution is compared to the finite element solutions discussed in this paper.

4.2 Measurement of Delamination Stresses

4.2.1 ANSYS Input

Again, ANSYS was used for the finite element solution. The physical model is identical to that used for the determination of the CTE and residual stresses as in Figure 2.10. Input data is similar to Figure 2.9. No temperature loads were imposed and a constant positive unit axial strain was imposed through the "D" boundary condition commands.

4.2.2 ANSYS Results

Figures 4.1 and 4.2 are the inplane and out-of-plane stress states through the thickness of the outer tension laminate for an average tested strain of 1.5%. In all graphs, the squares and pluses represent ANSYS results while diamonds and triangles represent the closed form TDCYL2 results obtained from the residual stress analysis discussed in Chapter 3. The abbreviations "gl0", "gl20", and "gr20" represent the glass hoops, glass helicals, and graphite helicals respectively. The vertical solid lines in the graphs represent the interlayer boundaries between these three different types of windings and materials. The dashed lines are the boundaries between $+\theta$ and $-\theta$ helical plies.

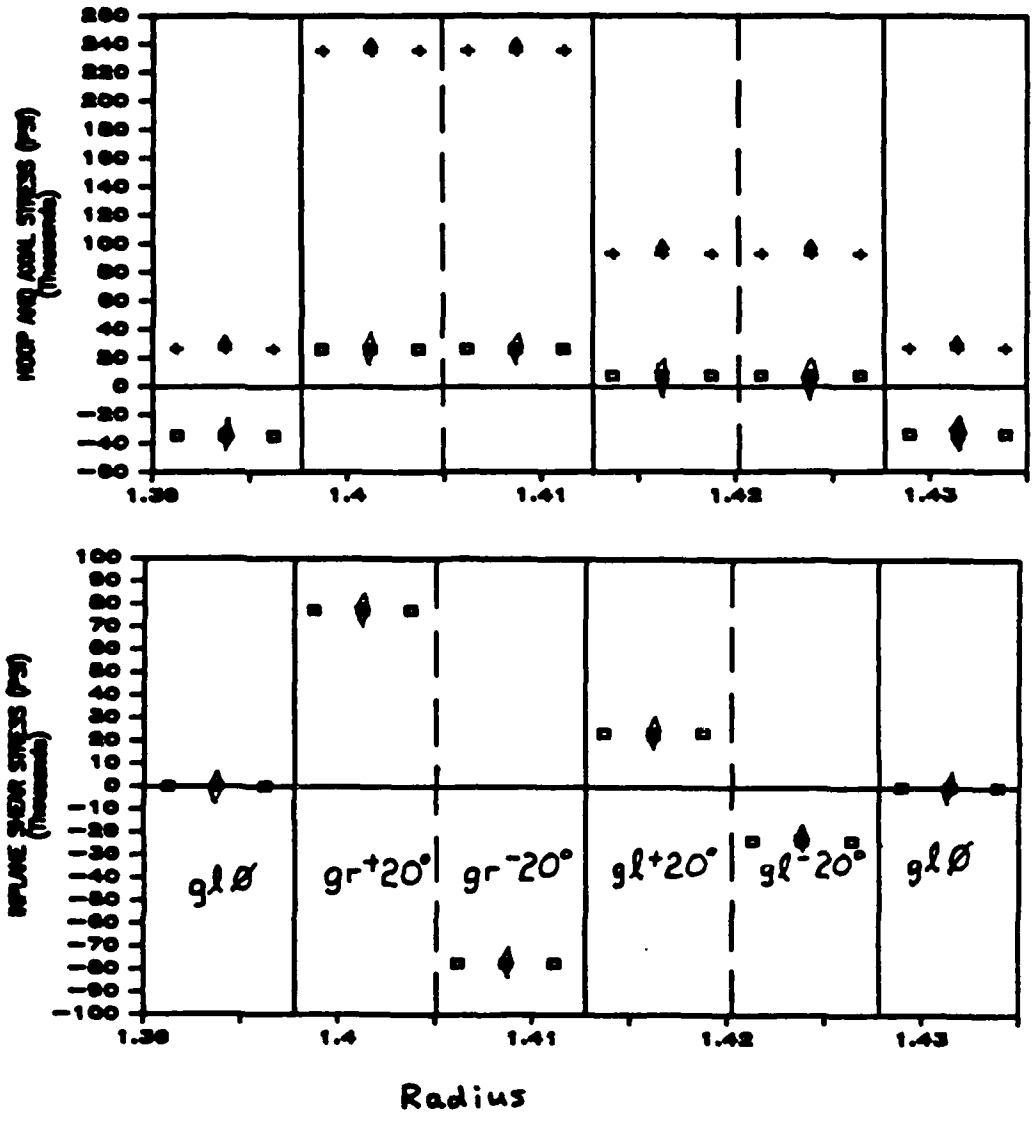

Figure 4.1 -- Inplane stress results from ANSYS (squares and plusses) and TDCYL2 (diamonds and triangles).

Considering only ANSYS results at this time, the squares in the top graph of Figure 4.1 indicate the hoop, or circumferential, stresses as predicted by ANSYS at the time of massive failure in the specimen (as opposed to matrix cracking which occurs somewhat earlier). The plusses, then, represent

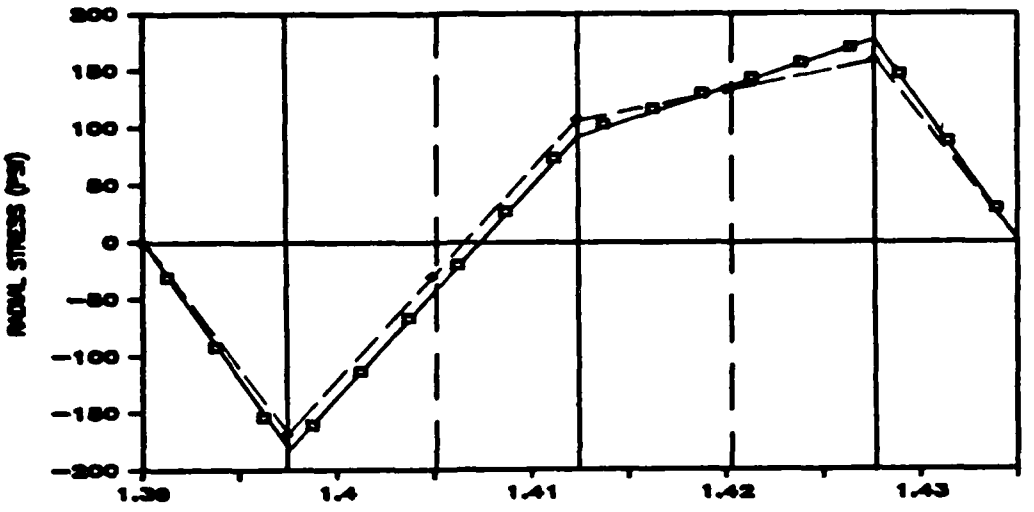

Figure 4.2 -- Out-of-Plane stress results from ANSYS (solid lines) and TDCYL2 (dashed lines).

the meridional, or axial, stresses at failure. As expected, these stresses are highest in the graphite helicals and lowest in the glass hoops. The lower graph of Figure 4.1 is the inplane shear (circumferential-axial) through the thickness. The actual analysis of these stresses with the failure allowables available in literature and the prediction of modes of failure is left to Foral and Gilbreath in their continuing research and upcoming publications.

4.2.3 Radial Delamination Problem

The interest here is in the out-of-plane radial stresses as predicted by ANSYS in the graph of Figure 4.2. In the experimental work, delamination failures were observed to occur consistently in the interlaminar region between the graphite helicals and glass helicals. The purpose here is to characterize the radial stresses present at this point and determine their ability to cause failure in tension normal to

the surfaces of the plies.

To obtain the best prediction of the actual stress state we need to superimpose the residual stresses due to fabrication determined in Chapter 3. Figure 4.3 is this superposition for radial stress through the thickness.

From Figure 4.3, the radial stress between the glass helicals and the outer glass hoop ply is larger than between the glass and graphite helicals where failure occurred. This may be evidence that a pure radial stress could not have caused the delamination failure.

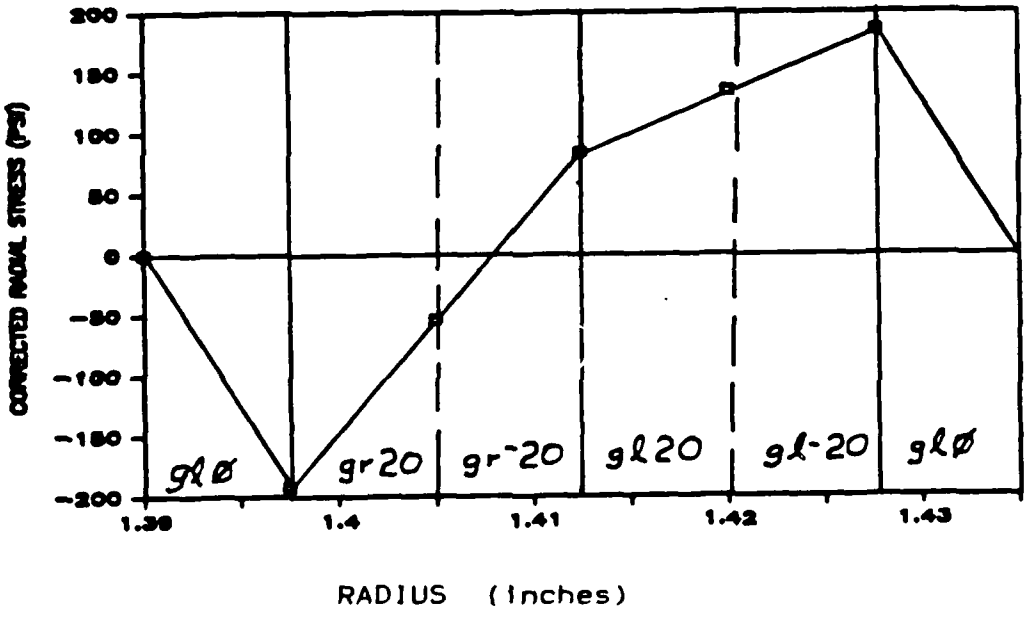

Figure 4.3 -- Radial stresses from ANSYS and TDCYL2 with residual stressses included.

This problem leads to Foral and Gilbreath's[2] work in failure mode determination. There may necessarily be a more complex mode of failure involving many more variables.

foral's work in "pullout" of fibers may give insight into this problem.

4.2.4 End Discontinuities

According to Waltz and Vinson[27], very little change is noted in the interlaminar normal stress (actually a slight decrease) in moving from the test section of the cylinder to the end discontinuities (loading grips).

The failures observed in the cylinders discussed in this paper do not appear to have progressed into the region of load or structural discontinuity. Using a relation by Vinson and Sierakowski[14] we can approximate the distance, d, from the grip in the specimen. The relation for d is,

$$d = 4\sqrt{Rh(D_x/D_\theta)^{1/2}} \qquad (4\text{-}1)$$

where R is the average radius of the cylinder, h is the thickness, D_x is a term for the axial stiffness, and D_θ is a term for the circumferential stiffness (eqn.s 4-2 and 4-3).

$$D_x = \sum_{k=1}^{n} \bar{Q}_{x_k} (t_k^3/12 + t_k d_k^2) \qquad (4\text{-}2)$$

$$D_\theta = \sum_{k=1}^{n} \bar{Q}_{\theta_k} (t_k^3/12 + t_k d_k^2) \qquad (4\text{-}3)$$

For the outer tension specimens being discussed here, d is evaluated to be 0.92 inches. An attempt was made to model this region in ANSYS. To maintain the appropriate boundary conditions it is necessary to model the portion of the cylinder from the end boundary conditions to a point in the membrane test section. Ideally, the entire half of the cylinder

would be modeled. However, just one and one-half inches of cylinder length resulted in more elements and nodes than the university version of ANSYS could maintain. Very small elements are necessary to model the various layers and an aspect ratio as high as 1:10 was attempted with no success. Substructuring methods were also done in an attempt to reduce the number of elements. Some ground was gained in this attempt. Computer time and restraints make work with this program very tedious and expensive.

Another method of finding these out-of-plane shear stresses would be to solve the 5*6=30 simultaneous differential equations (Waltz-Vinson[27]) in full form. Programs such as TUTSIM and TK SOLVER could be used to solve these equations. This work was out of the realm of this paper but may prove to be worthwhile in continued research.

Regardless of any future determination of the mode of failure that caused the delamination, characterizing the radial strength of these particular filament wound specimens is necessary. This is the purpose of the next section.

4.3 Allowables Testing

The need for bench tests to determine out-of-plane normal strengths of composite laminate cylinders has been established. Two tests were developed and run in a step toward this goal. (Refer to Figures 4.6 and 4.15 for diagrams of the apparatus for each test.)

4.3.1 Half-Ring Bench Test

The following is the process and the calculations used to determine the radial stresses given a measured hoop strain due to a change in curvature in the hoop direction. The physical process of measuring this strain is described in the next section.

4.3.1.1 Theory

The radial stress will be determined for the interlaminar region between the graphite and glass helicals since this is where failure was observed to occur. Using the program MATL[21], a unit moment was input to calculate, using general laminate theory, the inside strain and change in curvature on an outer tension cylindrical specimen.

(Note: Assume all values have a "y" subscript to denote the hoop direction. The subscripts "act" and "matl" refer to the actual measured values and the values calculated by the program MATL[21] respectively.)

INPUT: $M_{matl} = -1$ in-lb/in

OUTPUT: ϵ_{matl}

ΔK_{matl}

By the linear relationship between applied moment and resulting strain,

$$M_{act}/M_{matl} = \epsilon_{act}/\epsilon_{matl} \qquad (4\text{-}4)$$

Solving for the actual moment, M_{act}

$$M_{act} = -\epsilon_{act}/\epsilon_{matl} \qquad (4\text{-}5)$$

By the linear relationship between moment and curvature,

$$\Delta K_{act}/\Delta K_{matl} = M_{act}/M_{matl} \qquad (4\text{-}6)$$

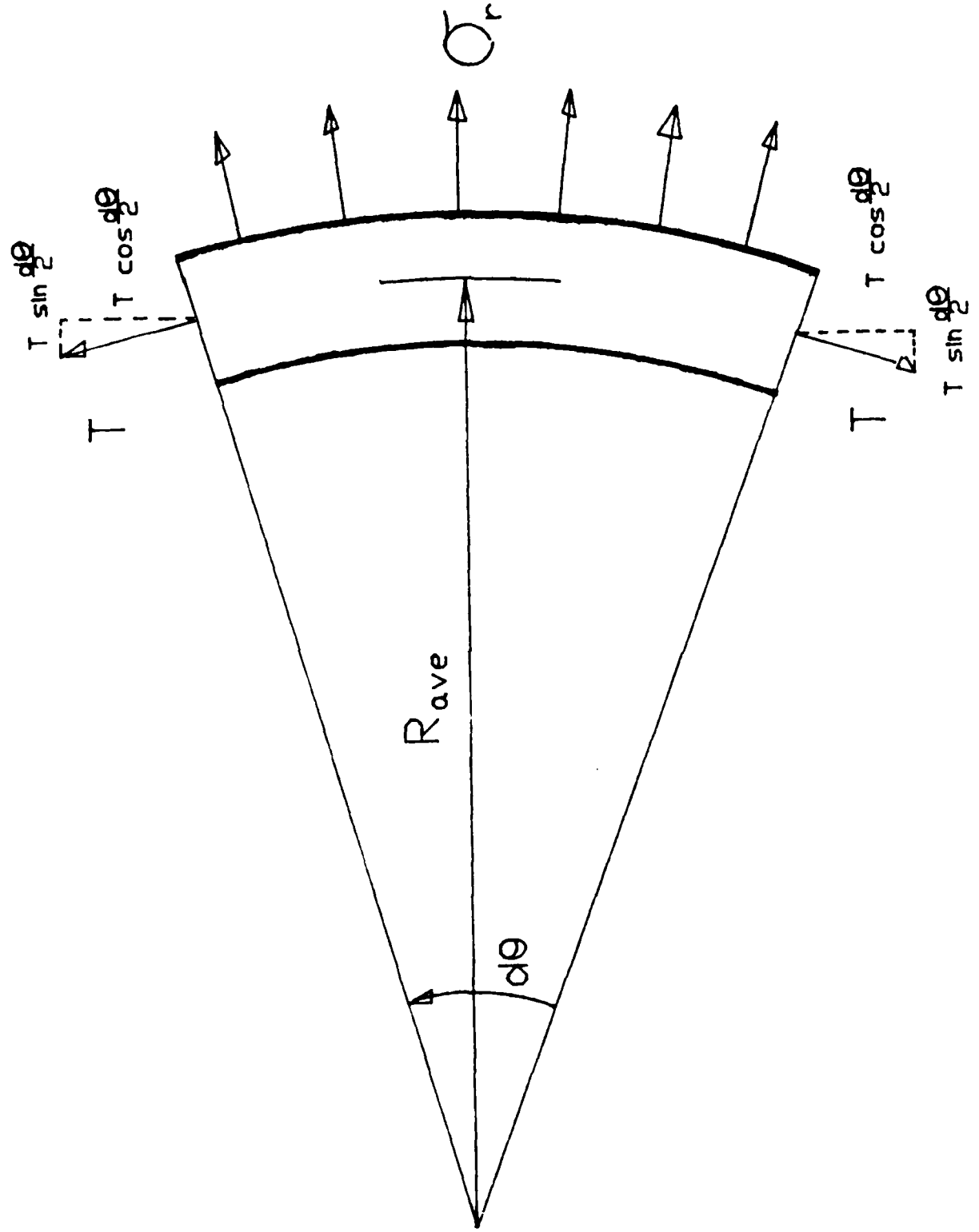

Figure 4.4 -- Radial Stress determination.

and solving for actual change in curvature, ΔK_{act},

$$\Delta K_{act} = -\Delta K_{matl} M_{act} \qquad (4\text{-}7)$$

Now substituting (4-5) into (4-7),

$$\Delta K_{act} = \Delta K_{matl} * \epsilon_{act}/\epsilon_{matl} \qquad (4\text{-}8)$$

The actual curvature can now be used to determine the radius of the specimen at any measured value of strain at the point of placement of the strain gage. From the definition of curvature,

$$\Delta K_{act} = 1/R_o - 1/R_f \qquad (4\text{-}9)$$

where R_o and R_f are the initial and final inner radii respectively. Solving for R_f,

$$R_f = R_o/(1-\Delta K_{act} R_o) \qquad (4\text{-}10)$$

The radius of curvature is now known and only the hoop stresses are needed to find the radial stress as shown in Figure 4.4 . From the strain distribution taken from MATL[21] we can get the average strains for the two layers involved as percentages of the measured hoop strains. Let a and b be these percentages in decimal form for the glass and graphite layers respectively. Thus,

$$\epsilon_{AVEgl} = a\epsilon_{act}$$
$$\epsilon_{AVEgr} = b\epsilon_{act} \qquad (4\text{-}11)$$

where "gl" and "gr" refer to the inside glass hoop ply and the graphite helical plies respectively. From general laminate theory, the hoop stresses in the layers can now be solved for,

$$\sigma_{gl} = \bar{Q}_{22gl}\epsilon_{AVEgl}$$
$$\sigma_{gr} = \bar{Q}_{22gr}\epsilon_{AVEgr} \qquad (4\text{-}12)$$

where $\bar{Q}_{22gl}$ and $\bar{Q}_{22gr}$ are constant material values taken

from MATL[21].

Now, referring to Figure 4.4 and summing forces in the z-direction,

$$\sigma_r(R_{AVE}d\theta) = 2[T\sin(d\theta/2)] \qquad (4\text{-}13)$$

By small angle approximations and solving for σ_r,

$$\sigma_r = T/R_{AVE} \qquad (4\text{-}14)$$

For this problem (see Figure 4.5),

$$T = \sigma_{gr}t_{gr} + \sigma_{gl}t_{gl} \qquad (4\text{-}15)$$

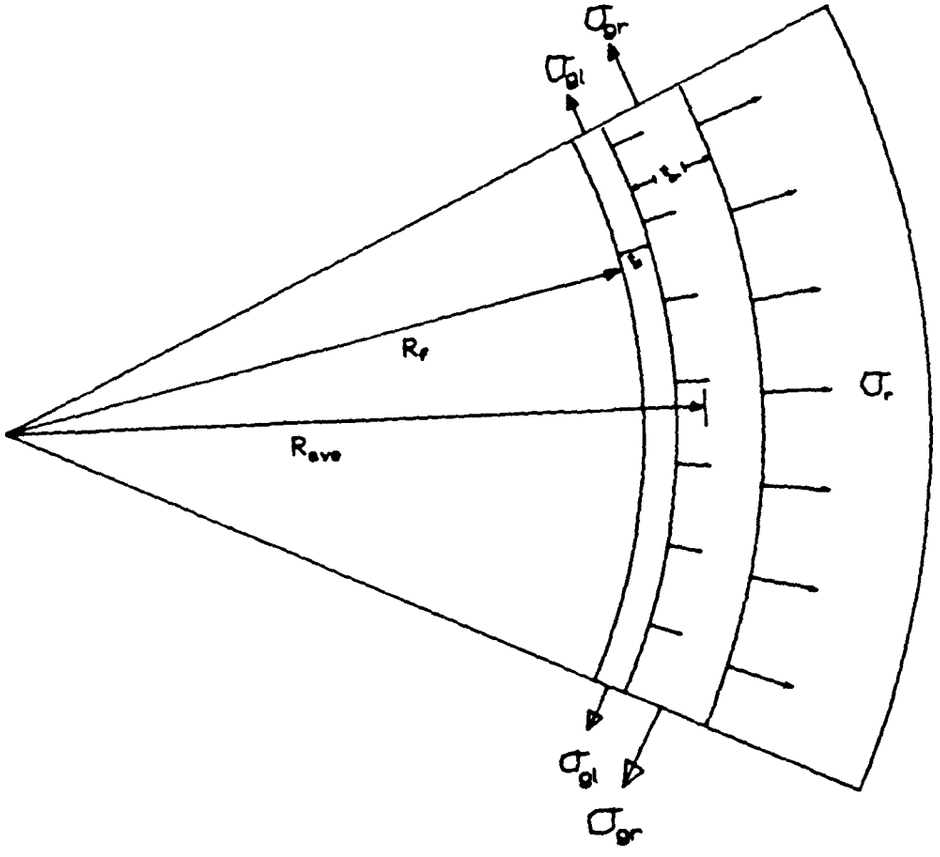

Figure 4.5 -- Radial stresses for outer tension specimen.

and,

$$\sigma_r = (\sigma_{gr}t_{gr} + \sigma_{gl}t_{gl})/R_{AVE} \qquad (4\text{-}16)$$

where t_{gr} and t_{gl} are the thicknesses of the respective

layers and,

$$R_{AVE} = R_f + (t_{gr} + t_{gl})/2 \qquad (4\text{-}17)$$

This radial stress can then be calculated once the strain at failure is measured.

4.3.1.2 Test Apparatus

Figure 4.6 is a schematic of the testing jig and apparatus used to produce a y-moment (and a transverse shear as discussed later) and, thus, a strain on the inner layer of

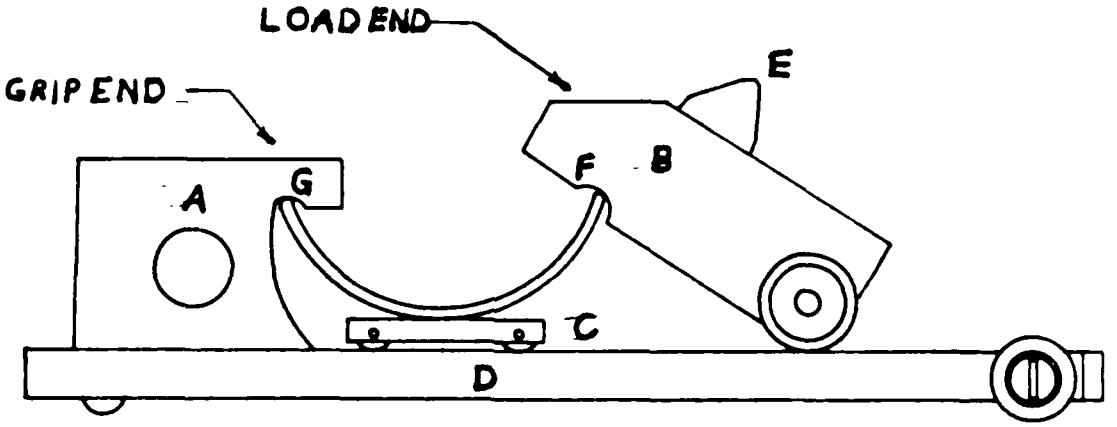

Figure 4.6 -- Test Jig for Half-Ring Delamination Test.

the half-ring specimen. Grip block "A" is securely fastened to plate "D" which is free to translate and rotate about its plane. Block "B" is free to translate away from block "A" as the specimen flattens out under the load at point "E". Block "C" was used simply as a spacer and was not allowed to translate during these tests. The specimen floats freely at points "G" and "F" as point "F" deflects. The variable distance between the load point "E" and the actual load point on the specimen, "F", is accounted for in the

results. The test jig is constructed almost entirely of aluminum.

4.3.1.3 Test Procedure

The procedure to measure the strain on the inside layer is as follows:

First rings are cut from the center "test section" portion of the cylinder. Half-rings of width 3/4" to 1-3/4" were tested in the jig and could not induce delamination. Next, rings were cut from the end "grip section" portions of the cylinder. Half-ring specimens from this thicker ring (see Table 4.1) tested well in the jig, delaminating in several specimens in the vicinity of point 1 in Figure 4.7 and continuing toward the grip end.

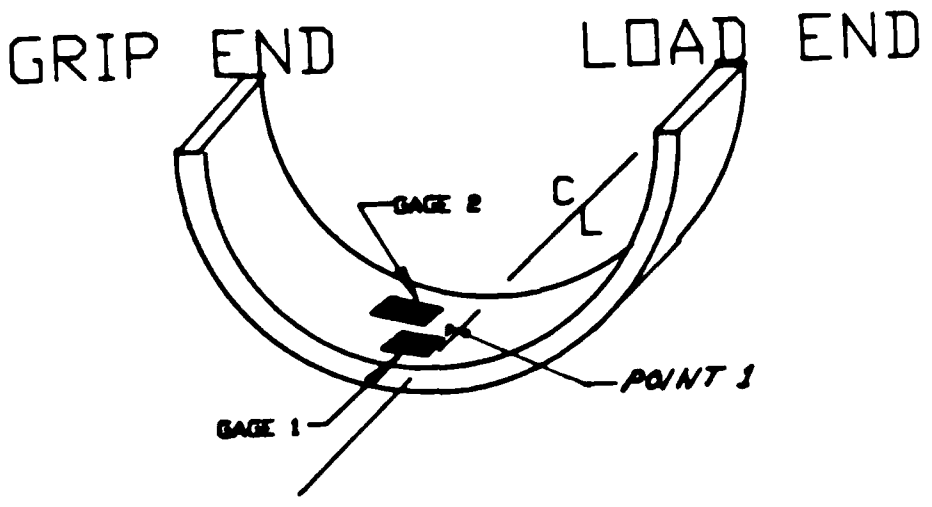

Figure 4.7 -- Gage Placement on Specimen.

Four specimens were cut from two 3/4 inch rings taken from one end of an outer tension specimen. The outer specimens were wound, from inside to outside, as shown in

Table 4.1. Property values for the 181 glass cloth were taken from Military Handbook 17[22]. The ring test to determine residual stresses in the specimen were conducted as described in Chapter 3.

It was desired to measure the strain in the vicinity of the failure so strain gages were placed as shown in Figure 4.7. The gages used were the same variety used in all previous testing and the method of placement is detailed in Micro-measurements Bulletins B-129-2[9] and B-127-9[10].

Layer	Thickness	Wind Angle	Material
1	0.00746	90	S-2/LRF-205
2	0.00746	20	AS-4/LRF-205
3	0.00746	-20	"
4	0.00765	20	S-2/LRF-205
5	0.00765	-20	"
6	0.00746	90	"
7	0.01	--	181 GLASS CL./LRF-205
8	0.0549	90	S-2/LRF-205
TOTAL=0.110			

Table 4.1 -- Laminate configuration of built-up ends on tension specimens.

Testing was done on a 60,000 pound Baldwin test machine at a load rate of approximately 100 pounds per minute. Maintaining a constant load rate was nearly impossible due to the variability of the specimens' ability to absorb energy as deflection progressed.

4.3.1.4 Test Results

In the following paragraphs, each half-ring delamination test is discussed with relevant information and results. The four specimens tested were arbitrarily labeled A2, A3, B2, and B3 with the A specimens being two halves of an original

ring specimen and likewise for the B specimens.

Specimen A2 was loaded with as constant a load with respect to time as possible. Considering the scale of the load dial on the 60,000 pound Baldwin the load vs. time graph of Figure 4.8.a appears to be fairly linear. The rate of strain with respect to load did not change appreciably throughout the test indicating a constant absorption of energy by the specimen as seen in Figure 4.8.b. Specimen A2 failed in sudden delamination at approximately 179 pounds with extrapolated strains of 0.0215 and 0.0170 for gages one and two respectively. Following delamination the residual load supported by the specimen was 65 pounds.

NOTE: The extrapolation was necessary due to the inability to take a reading at the point of failure.

Specimen A3's strain vs. time graph (Figure 4.9.c) indicates a fairly constant deflection as opposed to a constant load (Figure 4.9.a). This enables us to witness how load rate changes and, most importantly, how the load-strain curve changes. As the load-strain graph (Figure 4.9.b) shows there is a definite change in the rate at which strain occurs for a given load. This indicates that at loads above approximately 80 pounds this specimen requires less energy to deflect. Specimen A3 failed in sudden delamination at approximately 139 pounds with extrapolated strains of 0.028 and 0.024 for gages one and two respectively. Following delamination the residual load supported by the specimen was 55 pounds.

Specimen B2 follows the same pattern as specimen A3. The

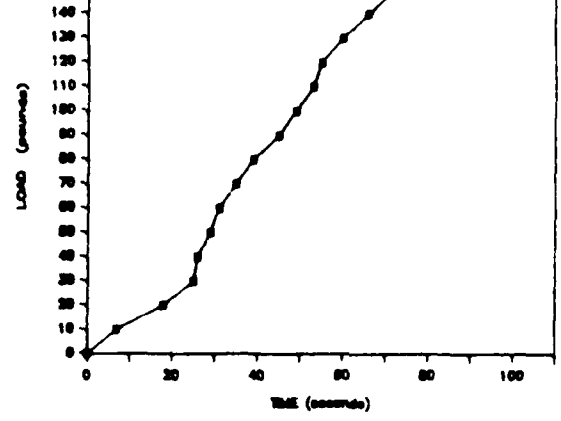

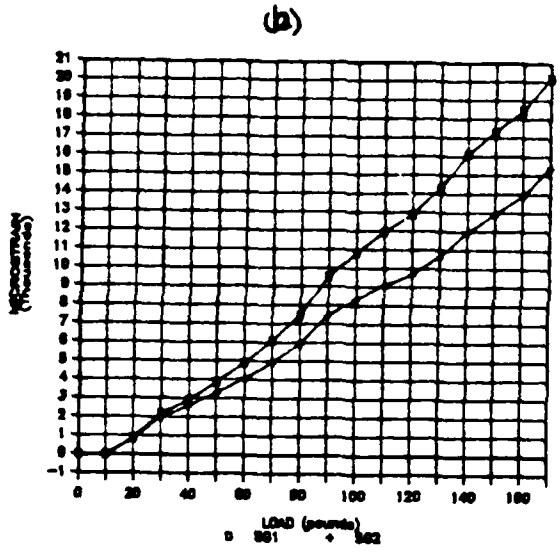

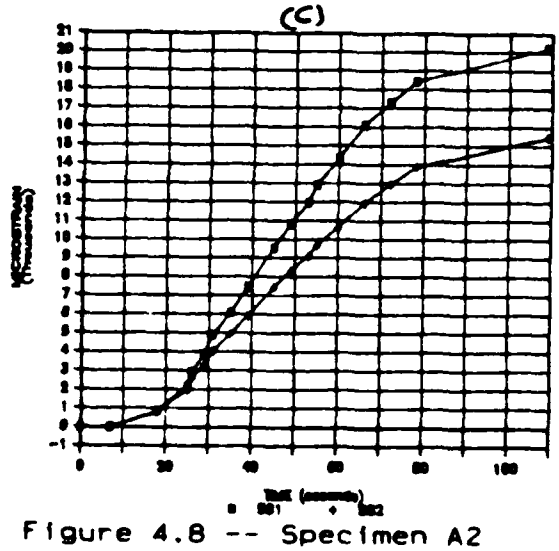

Figure 4.8 -- Specimen A2

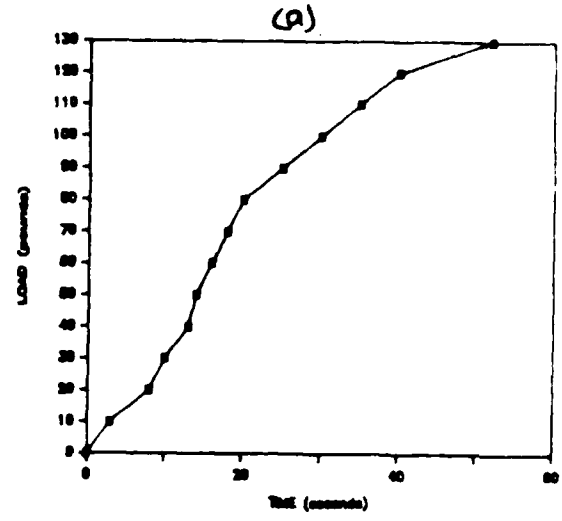

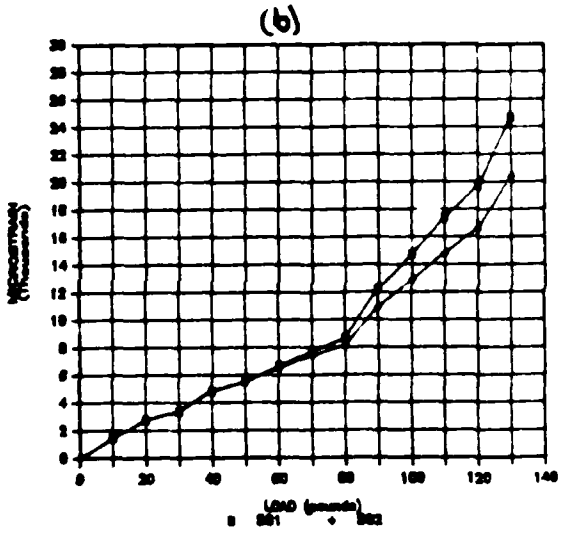

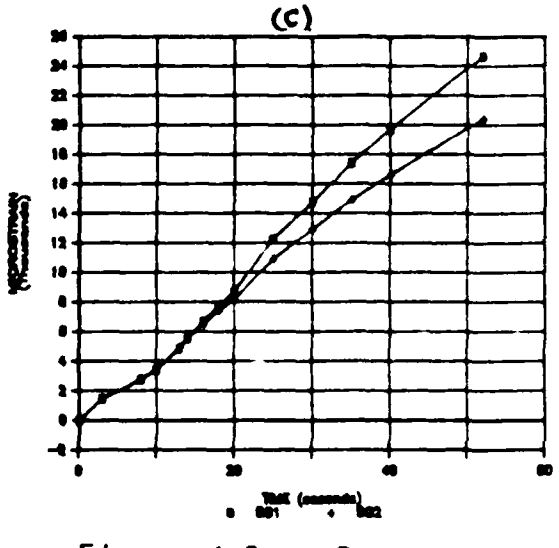

Figure 4.9 -- Specimen A3

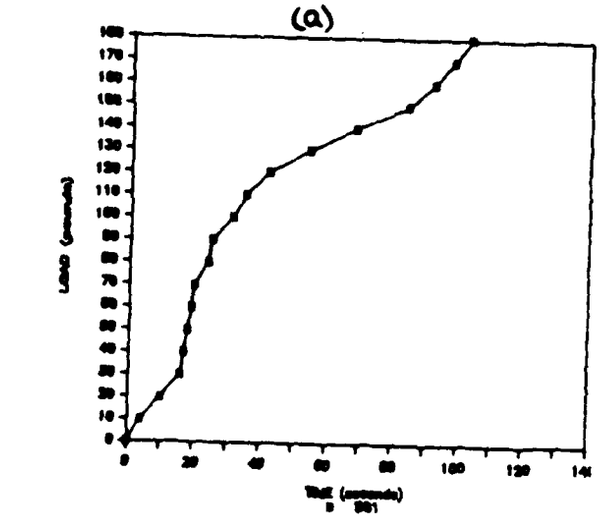

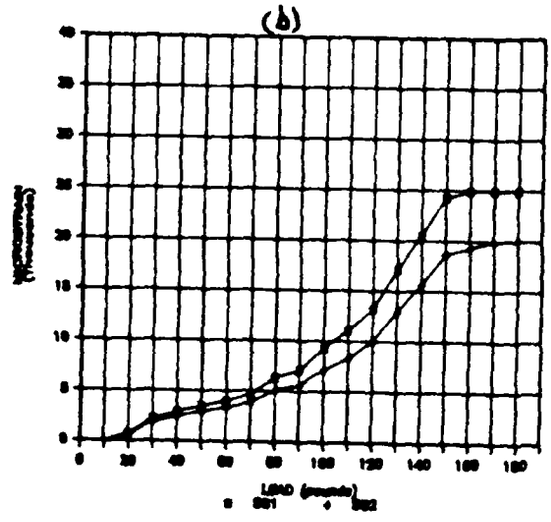

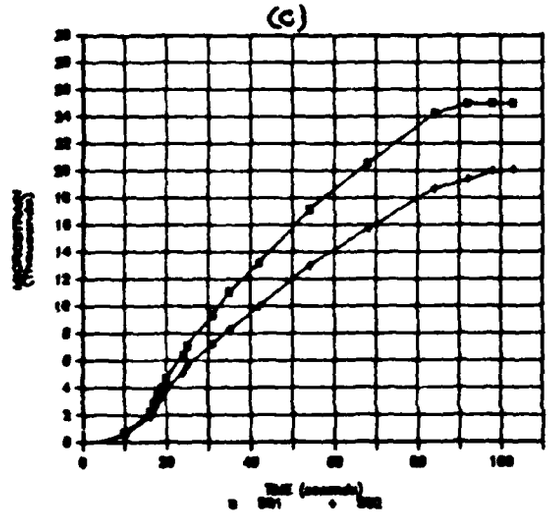

Figure 4.10 - Specimen B2

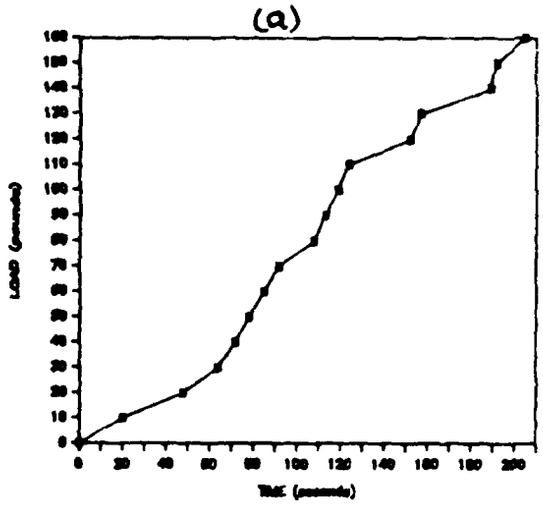

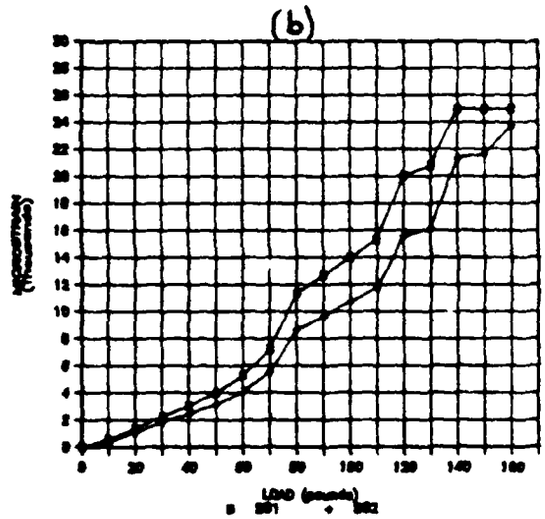

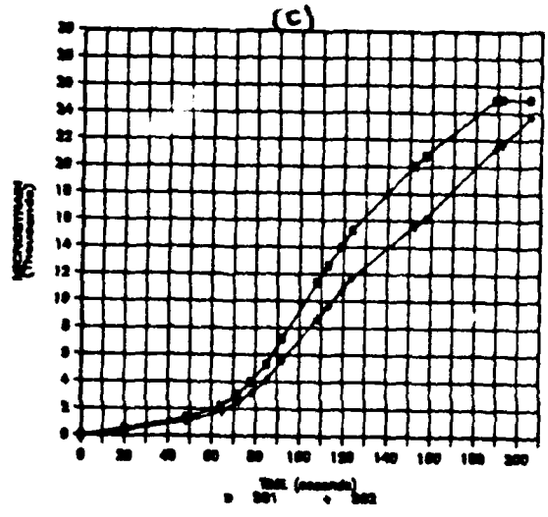

Figure 4.11 - Specimen B3

strain-time graph (Figure 4.10.c) shows a nearly linear path and the load-time graph (Figure 4.10.a) shows an obviously nonlinear path. The apparent nonlinear portion of the time-strain curve is due to the full scale setting of 25,000 microstrain on the strain indicator. Again, notice the obvious change in slope of the load-strain curve in Figure 4.10.b. Although the change is less sudden there is a definite decrease in stiffness of the specimen as it begins to take smaller increases in load to achieve the same deflections. Specimen B2 never failed in delamination as it reached a load of 190 pounds and deflected to a point of being completely flat.

Specimen B3 was tested completely by using the crank on the testing machine to load the specimen at two levels of constant deflection (Figure 4.11.c). This method allowed us to witness pauses in the load rate more accurately. As the load-time graph of Figure 4.11.a shows, there were pauses at 70, 110, 130, and 150 pounds. As the specimen reached each of these four loads the load actually dropped back 10-15 pounds before continuing under constant deflection. The load-strain curve of Figure 4.11.b better shows this lag in load required to produce strain. This specimen reached 165 pounds before failing in sudden delamination. It reached strains of approximately 0.030 and 0.026 respectively for gages one and two. The specimen supported a residual load of 65 pounds following failure.

Using the analysis above, Table 4.2 was obtained showing calculated radial stresses for each specimen not includ-

ing residual stresses. The calculated residual stresses in these specimens were found to average -28.4 +/- 2.0 psi in the interlaminar region between the graphite and glass helicals.

Specimen	Max Strain at Failure	Final Inside Radius (in)	Radial Stress at Failure (psi)
A2	0.0215	2.476	630.2
A3	0.0280	3.285	619.2
B2	--	--	--
B3	0.0300	3.652	597.0
			MEAN=615.5
			CoC=0.027

Table 4.2 -- Results of half-ring delamination test.

4.3.1.5 Analysis of Results

Table 4.3 gives the midplane stresses in the hoop (circumferential) direction corresponding to the measured strains for specimen B3 (also characteristic of specimens A2 and A3). These stresses include the calculated residual stresses determined earlier for the thickened specimens.

Layer	Mid-layer stress (psi)	Load Carried (lb)
glass hoop	217,774	1218.0
graphite +20	28,987	162.2
graphite -20	24,974	139.7
glass +20	33,818	194.0
glass -20	27,271	156.5
glass hoop	84,110	470.6
glass cloth	22,123	165.9
glass hoop	-61,211	-2520.4
		Total = 0

Table 4.3 -- Midlayer stresses and loads through the thickness of specimen B3 at the point of failure.

The stresses in Table 4.3 are very close to failure

stresses for various layers. For instance, the glass hoops have a strength of 230 ksi[23] which is just slightly above the 217.8 ksi experienced by the inside hoop layer. The glass and graphite helicals are nearly double their usual ultimate transverse stress levels and probably experienced some cracking.

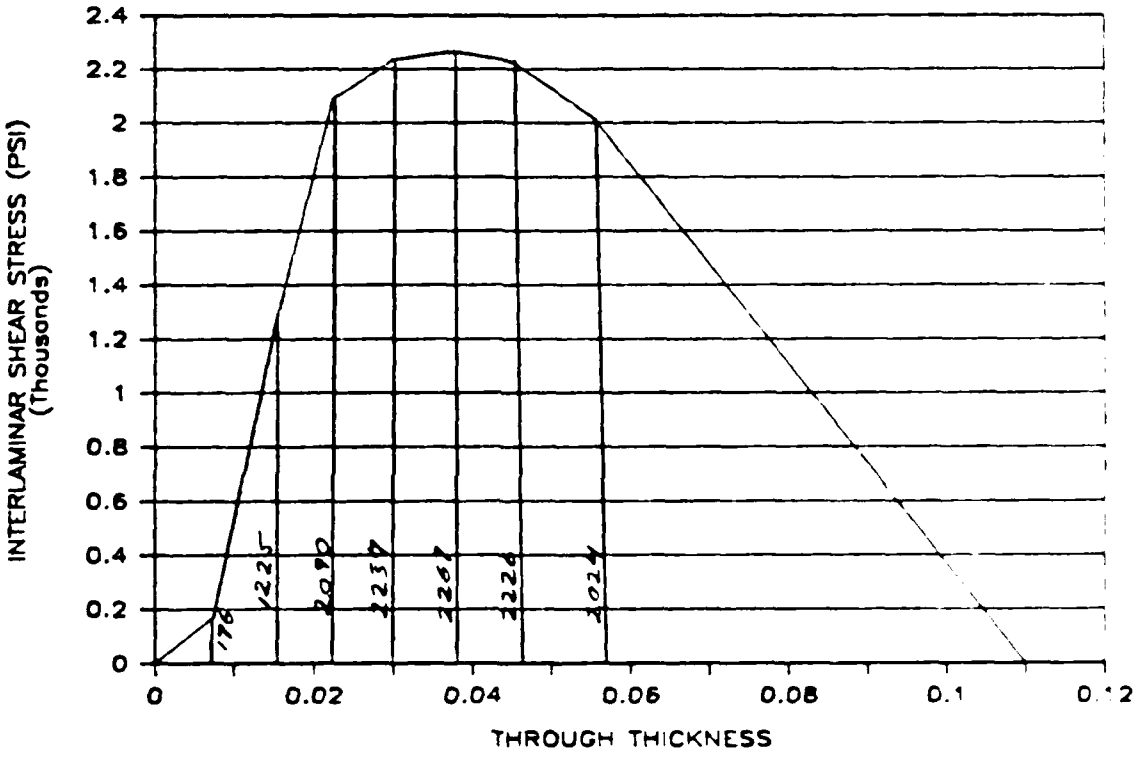

Figure 4.12 -- Interlaminar shear stress distribution.

Figure 4.12 shows the distribution of the radial-circumferential interlaminar shear stress at the point of ure in the half-ring tests. This distribution was found from the known transverse load applied to the specimen. The maximum shear stress of 2.3 ksi is well below common allowables[23] for interlaminar shear stress in these materials. Again, the allowable may be somewhat lower than expected

resulting in a delamination of the specimen due to transverse load and interlaminar shear.

To get rid of the transverse load and thus the high shear, it is tempting to come up with a method to apply a pure moment to the half-ring specimen. This would result in only normal radial stresses in the out-of-plane delamination-causing stresses. However, returning to the theory used to reduce the measured strain to radial stresses and plotting calculated radial stress against measured strain for the entire possible deflection (flattening out) of the half-ring specimen, we see that the maximum possible radial stress for this thickness and material stacking sequence is about 630 psi (Figure 4.13).

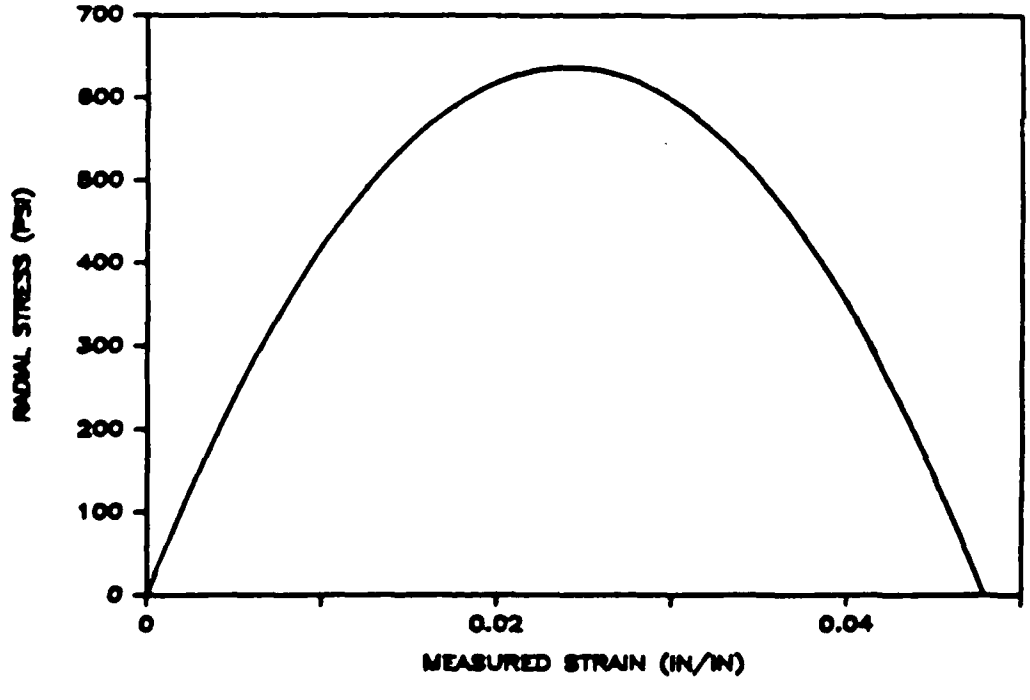

Figure 4.13 -- Radial Stress vs. Inside Strain from Theory for Outer Tension Specimens.

This level of radial stress is reached before delamination occurs, indicating that the radial stress allowable must be higher than 630 psi. Another means of determining this allowable must be investigated.

Using the Chang-Springer[24] failure criteria for fiber reinforced composite bends, the problem may become clear. Figure 4.14 indicates this failure envelope with the solid line being the envelope representing the commonly used values[23] for interlaminar shear and normal allowables in epoxy resin based laminates. The circles represent the values of shear and radial stresses calculated by the half-ring test. The single square symbol is a result obtained from the coupon bench test discussed in the next section.

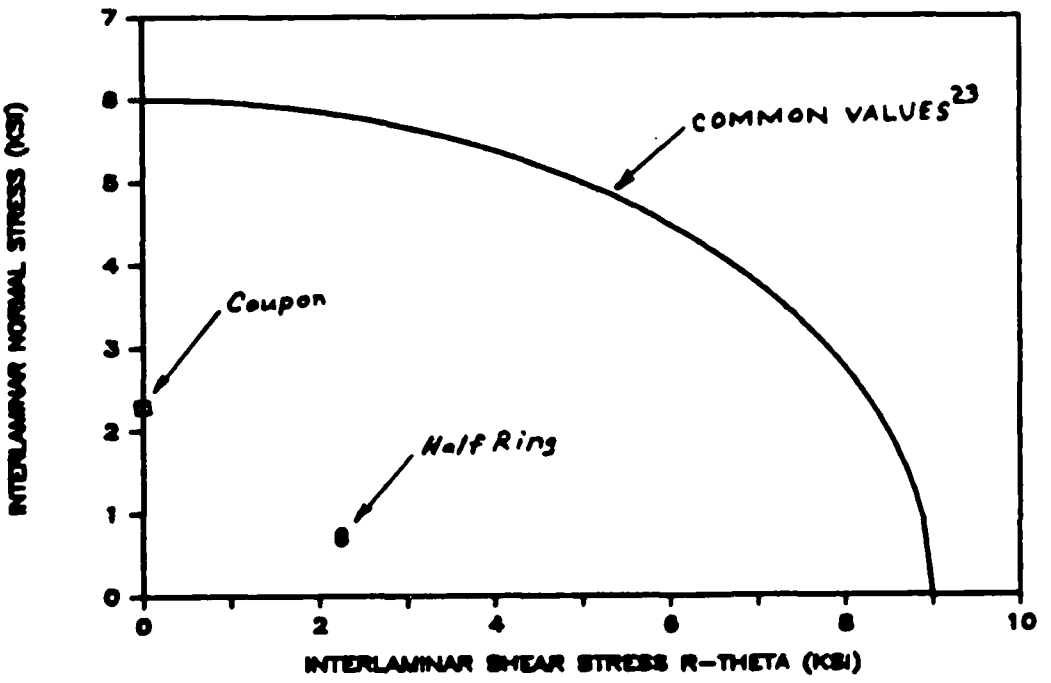

Figure 4.14 -- Chang-Springer Failure Envelope.

4.3.2 Coupon Bench Test

4.3.2.1 Introduction

The goal of this test is to apply a direct tensile delaminating load to a small section of our specimen. Lagace and Weems[17] tested AS4 graphite/epoxy in out-of-plane tension. They used a thick (12-13 mm) laid up laminate specimen necked down in the test section. The specimen was bonded to aluminum grips which could provide stabilization of the specimen and apply the out-of-plane tensile load. The necking down of the test section allowed them to produce a higher stress in the plane of desired failure than in the plane of adhesive bonding. Lagace and Weems[17] were able to produce good data with an average through-the-thickness strength of 6.24 ksi.

A shortcoming of this method involves the fabrication of the specimen and its thickness. The specimen laminate may not have been laid up with the same standards as the materials for which this type of information is sought. Perhaps test specimens were laid up with different thicknesses, different pressures applied, different cure cycles, or even different fabrication techniques such as filament winding. These variables could change the through-the-thickness strength of applicable composites.

The goal of the coupon bench test is to develop this same principle to work for coupons cut from filament wound composite cylinders, namely, those being tested here. Test specimens were only about 1.1 and 2.8 mm thick for the test section portion of the test cylinder and the end sections per

tions respectively. This small thickness would not allow a necking down in the "test section" of the coupon. Therefore failures near the load discontinuities under tensile loading would be possible and may cause premature failure. The value of this test is that it can provide a pure radial stress allowable providing failure occurs away from harmful discontinuities or if the discontinuity effects are small. If failures occur in the test section of the coupon, then we have a specific allowable. If failure occurs near the ends where end discontinuities are in effect, the test still provides a usefull lower boundary to the radial stress allowable.

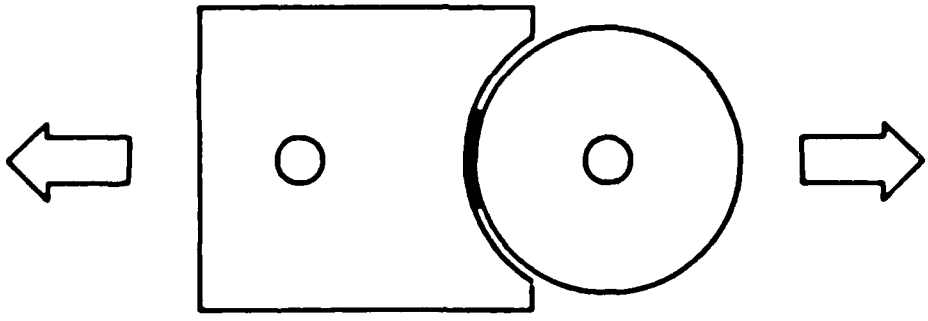

Figure 4.15 -- Test Jig for Coupon Bench Test.

4.3.2.2 Testing Apparatus and Procedures

Figure 4.15 indicates the loading grips that were machined specifically for laminates of these radii and thicknesses. The half-inch holes in each grip provide both loading points and mobility of the specimen to reduce any possible damaging moments within the specimen. The grips were machined from aluminum with the "square" grip having radius

on its concave surface equal to the outer radius of the half-ring specimen. The round grip was machined with a radius equal to the inner radius of the specimen. The thickness of the grips was cut and milled to 0.723 inches. Specimens were carefully cut with a bandsaw to avoid fraying of the ends. Final specimens ranged from 0.71 to 1.02 inches wide. The second planar dimension of the coupon was that of the grips since they were sanded flush to the surface of the jig after bonding.

Bonding was done in a jig which supported both grips to a plate with a set screw to tighten the grips together through the plane of the coupon. The coupon was centered in the jig by sight using hash marks scribed into the surface of the "square" grip. 3M Scotch-Weld DP-110 clear epoxy adhesive was used for bonding. The surfaces were prepared using methyl ethyl ketone as a cleaning agent on the aluminum and the normal surface preparation techniques for applying the strain gages in earlier tests. The adhesive is fast setting and flexible with a manufacturer's claim of 2500 psi shear strength. No values of normal strength were given. From 48 to 72 hours set time is recommended.

4.3.2.3 Test Results

Five tests were completed as time allowed. Four thickened end coupons and one thinner test section coupon were tested. Table 4.4 shows the results of these tests including failure descriptions.

TEST #	SPEC. TYPE	FAILURE DESCR.	LOAD (LB)	AREA (in^2)	STRESS (PSI)
1	END	1	280	0.737	--
2	END	2	1020	0.690	1478
3	END	3	960	0.657	1462
4	END	2	1120	0.713	1571
5	MIDDLE	4	1130	0.513	2203

FAILURE DESCRIPTIONS:

1. Failed under impact due to error. Adhesive failure.
2. Clean failure in last outer glass hoop ply.
3. Clean failure between inner glass hoop and graphite helicals.
4. Clean failure between graphite and glass helicals.

Table 4.4 -- Results of Coupon Delamination test.

The failures in the end specimens may exhibit some load discontinuities, perhaps explaining their lower failure stresses. The failure in the one test-section specimen was exactly where actual delamination occurred in the original test cylinders. This failure stress of 2200 psi can then be plotted on the Chang-Springer[24] failure envelope of Figure 4.15. These results indicate a smaller failure envelope than Lagace and Weems[17] reported. Differences in this value among various laminates is certainly not inconceivable. The coupon tested from the test section of the cylinder had gaps in the winding pattern of the graphite helicals of approximately 15% as viewed in a Zeiss stereo microscope. These gaps certainly effect the radial strength of the material. The question arises whether or not one expects filament wound laminates to have lower transverse strengths than laid up laminates due to

a greater percentage of voids, wind tension, or other factors of the fabrication process. Questions like this must be answered before general allowables can be used with confidence.

Certainly, more tests are necessary to establish a data base upon which to draw conclusions. This test, however, does show some promise as a means of determining radial stress allowables in composite cylinders.

CONCLUSIONS

1. The general purpose proprietary finite element program ANSYS is a viable tool for the three-dimensional study of laminated composite cylinders. It is, however, costly and time consuming.

2. Linear coefficients of thermal expansion for filament wound laminates can be predicted using classical lamination theory.

3. Residual stresses in filament wound laminates can be predicted using classical lamination theory.

4. Progress toward practical normal delamination strength tests in cylindrical laminates has been achieved.

APPENDIX - STRAIN GAGE INFORMATION

Gage Type: EA-06-250BG-120

EA - General Purpose constantan strain gage

(EA is the series)

(the Micro-Measurements EA gage is like the BLH Electronics FAE)

1 mil (.03 mm) polyimide backing

temperature range -320 F to 400 F for dynamic testing.

STRAIN RANGE = +/- 5% FOR G.L. > 1/8"

E=open-faced general purpose, polyimide backing

A=constantan alloy in self-temperature-compensated form

06=the S-T-C (Self-Temperature-Compensation) number is the approximate thermal expansion coefficient in PPM/ F of the structural material on which the gage is to be used. 06 can be for 'A' alloys or 'K' alloys.

250=the active gage length in mils

BG= specifies Grid and Tab geometry

120=resistance in Ohms

gage length=6.35 mm

overall length=9.53 mm

grid width=3.18 mm

overall width=3.18 mm

matrix size=13.2mmL x 5.6mmW

See MM engineering data sheet for more information.

REFERENCES

1. Charles W. Bert, "Static Testing Techniques for Filament-Wound Composite Materials." Composites, January, 1974, pp. 20-26.

2. R.F. Foral, D.R. Gilbreath, and B.K. Fink, "Delamination Failure Modes in Filament Wound Composite Tubes," ASTM Second Symposium on Composite Materials: Fatigue and Fracture, April 27-28, 1987, Cincinnati, Ohio.

3. D.R. Gilbreath, Personal Communication, Fall, 1986.

4. C.C. Chamis, "Simplified Composite Micromechanics Equations for Hygral, Thermal, and Mechanical Properties," SAMPE Quarterly, April, 1984, pp. 14-23.

5. C.T. Herakovich, "Composite Laminates with Negative Through-the-Thickness Poisson's Ratios," Journal of Composite Materials, Vol. 18, September, 1984, pp. 447-455.

6. M.W. Poore and K.F. Kesterson, "Measuring the Thermal Expansion of Solids with Strain Gages," Journal of Testing and Evaluation, JTEVA, Vol. 6, No. 2, March 1978, pp. 98-102.

7. Measurements Group, Tech Note 513 -- Thermal Expansion Measurement, 1986.

8. M.B. Kasen, "Properties of Filamentary-Reinforced Composites at Cryogenic Temperatures," Composite Reliability, ASTM STP 580, American Society for Testing and Materials, 1975, pp. 586-611.

9. Measurements Group, Instructional Bulletin B-129-2, "Surface Preparation for Strain Gage Bonding," 1976.

10. Measurements Group, Instructional Bulletin B-127-9, "Strain Gage Installations with M-Bond 200 Adhesive," 1976.

11. M.L. James, G.M. Smith, and J.C. Wolford, Applied Numerical Methods for Digital Computation. New York: Harper & Row, Publishers, Inc., 1985.

12. R.M. Jones, "Mechanics of Composite Materials," Scripta Book Company, 1975.

13. S.W. Tsai, "Introduction to Composite Materials," Technomic Publishing Co., Inc., 1980.

14. J.R. Vinson and R.L. Sierakowski, The Behavior of Structures Composed of Composite Materials, Martinus Nijhoff Publishers, 1986, pp. 40-57.

15. W.T. Freeman and M.D. Campbell, "Thermal Expansion Characteristics of Graphite Reinforced Composite Materials," Composite Materials: Testing and Design (Second Con ASTM STP 497, American Society for Testing and Materials, 1972, pp. 121-142.

16. I.M. Daniel, "Thermal Deformations and Residual Stresses in Fiber Composites," Thermal Expansion 6, Ian D. Peggs, Editor, Plenum Press, New York, 1978, pp. 203-222.

17. P.A. Lagace and D.B. Weems, "A Through-the-Thickness Strength Specimen for Composites," Technical Lab for Advanced

Composites Report, November, 1986.

18. T.V. Parry and A.S. Wronski, "Kinking and Tensile, Compressive and Interlaminar Shear Failure in Carbon-Fibre-Reinforced Plastic Beams Tested in Flexure." Journal of Materials Science, Vol. 16, 1981, pp. 439-450.

19. N.J. Pagano, "Stress Gradients in Laminated Composite Cylinders." Journal of Composite Materials, Vol. 5, April, 1971, pp. 260-265.

20. E. Reissner and W.T. Tsai, "On Pure Bending and Stretching of Orthotropic Laminated Cylindrical Shells." Journal of Applied Mechanics, March, 1974, pp. 168-172.

21. R.F. Foral and others, MATL, general laminate theory program written in FORTRAN, Department of Engineering Mechanics - University of Nebraska-Lincoln.

22. "Plastics For Flight Vehicles - Part 1: Reinforced Plastics," Military Handbook 17, Armed Forces Supply Support Center, Washington, D.C., 1959.

23. Class Notes, Engineering Mechanics 930, Composite Materials, Instructor: R.F. Foral, University of Nebraska-Lincoln, Spring, 1986.

24. F.K. Chang and G.S. Springer, "The Strengths of Fiber Reinforced Composite Bends," Journal of Composite Materials, Vol. 20, January 1986, pp. 30-45.

25. N.L. Newhouse, "Mechanical and Transient Hygrothermal loading of Multilayer Orthotropic Cylinders," PhD Dissertation, University of Nebraska-Lincoln, 1984.

26. G.Z. Voyiadjis, P.D. Kiousis, and C.S. Hartley, "Analysis of Residual Stresses in Cylindrically Anisotropic Materials," Experimental Mechanics, June, 1985, pp. 145-147.

27. T.L. Waltz and J.R. Vinson, "Interlaminar Stresses in Laminated Cylindrical Shells of Composite Materials," AIAA Journal, Vol. 14, No. 9, September, 1976, pp. 1213-1218.

END

2-87

DTIC